RNA Aptamer-Based Systems for Pathogen Detection and Biomolecule Synthesis

by

Anli Tang

A Dissertation Presented in Partial Fulfillment
of the Requirements for the Degree
Doctor of Philosophy

Approved November 2020 by the
Graduate Supervisory Committee:

Alexander Green, Chair
Hao Yan
Neal Woodbury

ARIZONA STATE UNIVERSITY

December 2020

ABSTRACT

RNA aptamers adopt tertiary structures that enable them to bind to specific ligands. This capability has enabled aptamers to be used for a variety of diagnostic, therapeutic, and regulatory applications. This dissertation focuses on the use RNA aptamers in two biological applications: (1) nucleic acid diagnostic assays and (2) scaffolding of enzymatic pathways. First, sensors for detecting arbitrary target RNAs based the fluorogenic RNA aptamer Broccoli are designed and validated. Studies of three different sensor designs reveal that toehold-initiated Broccoli-based aptasensors provide the lowest signal leakage and highest signal intensity in absence and in presence of the target RNA, respectively. This toehold-initiated design is used for developing aptasensors targeting pathogens. Diagnostic assays for detecting pathogen nucleic acids are implemented by integrating Broccoli-based aptasensors with isothermal amplification methods. When coupling with recombinase polymerase amplification (RPA), aptasensors enable detection of synthetic valley fever DNA down to concentrations of 2 fM. Integration of Broccoli-based aptasensors with nucleic acid sequence-based amplification (NASBA) enables as few as 120 copies/mL of synthetic dengue RNA to be detected in reactions taking less than three hours. Moreover, the aptasensor-NASBA assay successfully detects dengue RNA in clinical samples. Second, RNA scaffolds containing peptide-binding RNA aptamers are employed for programming the synthesis of nonribosomal peptides (NRPs). Using the NRP enterobactin pathway as a model, RNA scaffolds are developed to direct the assembly of the enzymes entE, entB, and entF from *E. coli*, along with the aryl-carrier protein dhbB from *B. subtilis*. These scaffolds employ X-shaped RNA motifs from bacteriophage packaging motors, kissing loop interactions from HIV, and peptide-binding RNA aptamers to position peptide-modified NRP enzymes. The resulting RNA scaffolds functionalized with different aptamers are designed and evaluated for *in vitro* production of enterobactin. The best RNA scaffold provides a 418% increase in enterobactin production compared with the system in absence of the RNA scaffold. Moreover, the chimeric scaffold, with *E. coli* and *B. subtilis* enzymes, reaches approximately 56% of the activity of the wild-type enzyme

assembly. The studies presented in this dissertation will be helpful for future development of nucleic acid-based assays and for controlling protein interaction for NRPs biosynthesis.

ACKNOWLEDGMENTS

I would first like to express my sincere gratitude and appreciation for my supervisor, Dr. Alexander A. Green, for his dedicated support, guidance, patience and encouragement. He has consistently aided in my journey in my graduate studies, and his knowledge in synthetic biology has been invaluable in helping me navigate my research on RNA aptamer applications.

I am grateful for the members of my committee Dr. Hao Yan and Dr. Neal Woodbury for their guidance throughout the past years. I would like to thank them for their valuable comments and inspiring advice on manuscript writing and data interpretation, and for taking the time for me on poster session weekends, every year in this six year process.

My thanks go to my current and formal lab members Soma Chaudhary, Zhaoqing Yan, Yuexin Li, Kaiyue Wu, Griffin McCutcheon, Kirstie Swingle, Sanchari Saha, Dr. Matthew Gilliam, Dr. Abhishek Debnath, and Dr. Ahmed Yousaf for their friendship and help over the years of my studies. I'd like to thank Dr. Duo Ma, Dr. Shuoxing Jiang and Dr. Minghui Liu for teaching me basic lab techniques when I first started my research.

Of course, I would like to thank my family and Ruoyang Zhang. My deepest gratitude goes to my parents and the rest of the family for their love, patience, support and encouragement. To my cousins who correct my grammar whenever I need them.

None of what has been accomplished in this piece would have been possible without the help of the people listed, or without the help of many others unmentioned. To the many others who have helped me move along inch by inch in this long journey, thank you.

TABLE OF CONTENTS

CHAPTER Page

CHAPTER Page

LIST OF FIGURES

CHAPTER 1

INTRODUCTION

1.1 RNA Aptamers as Diagnostics

RNA aptamers are short, single-stranded RNA molecule selected *in vitro* to recognize and bind targets with high affinity and specificity by folding into tertiary structures. The term aptamer[1] derived from the Latin '*aptus*', to fit. The method for RNA aptamer selection was developed 30 years ago[1,2], called systematic evolution of ligands by exponential enrichment (SELEX). The conventional SELEX cycle starts with the incubation of a library of RNA with a specific target, and the bound RNAs are separated from those that are unbound and then amplified by RT-PCR. The resulting cDNAs are used as templates, serving to enrich RNAs with high affinity for the next round of selection. The process is repeated until an RNA pool with highest affinity is isolated. This method can also be used for the selection of DNA aptamers; nevertheless, this chapter is focused on RNA aptamer and its applications. There are multiple variations of SELEX such as capture-SELEX[3], immunoprecipitation-coupled SELEX (IP-SELEX)[4], cell-SELEX[5], and *in vivo* animal SELEX[6]. These advancements permit the selection of aptamers against a widened range of targets, such as soluble small molecules, native state proteins, live cells and even live animals.

The diverse potential targets of RNA aptamers give rise to a great number of applications in diagnostics, biosensing, and therapeutics. By definition, the ability to recognize target with high affinity and specificity makes aptamers ideal as diagnostic agents for pathogens and cancer. RNA aptamers were selected for targeting viruses and parasites including hepatitis C virus[7,8], hepatitis B virus[7,8], influenza B virus[9], Severe Acute Respiratory Syndrome (SARS) coronavirus[10], *P. falciparum*[11], *T. brucei*[12], *and T. cruzi*[13]. Furthermore, RNA aptamers have been developed for the detection of cancer-related biomarkers including carcinoembryonic antigen (CEA), CA50, CA72-4 for gastrointestinal cancer[14].

1.2 RNA Aptamers Used in Biosensing.

The conformational change of the RNA aptamer upon binding to its specific target allows it to serve as a molecular switch. Aptamer-based biosensors, or aptasensors combine RNA aptamers with variety of readout methods, examples of fluorescence output is discussed here. In 2006, a simple fluorescent aptasensor was developed for theophylline (Fig. 1.1a)[15]. The ends of a single-stranded linear DNA was labeled with a fluorophore and a quencher, respectively. In absence of the target molecule, fluorescence signal increased upon binding with the RNA aptasenor. When the target molecule was present, it binds to the RNA aptamer. As result, the fluorescence decreased again. Researchers developed a Fluorescent Resonance Energy Transfer (FRET)-based theophylline aptasensor in 2009 (Fig. 1.1b)[16]. The RNA aptamer is inserted in a rev response element (RRE)-RNA, and Rev-peptide is inserted between EYFP and ECFP (EYFP-Rev-ECFP). When theophylline is present, RRE-RNA reconfigure and binds to the EYFP-Rev-ECFP. As result, the FRET signal increases. More recently, a fluorescence-based aptasensor was engineered that can detect histamine at a concentration of 1 μM (Fig. 1.1c)[17]. An RNA aptamer was fluorescently labeled at 5' end, and partially hybridized with a quencher DNA strand. The binding of the histamine to the aptamer displaces the quencher strand and increases the fluorescence. There are similar fluorescent-based RNA aptasensor designs by replacing the quencher with gold nanoparticle (AuNP)[18,19].

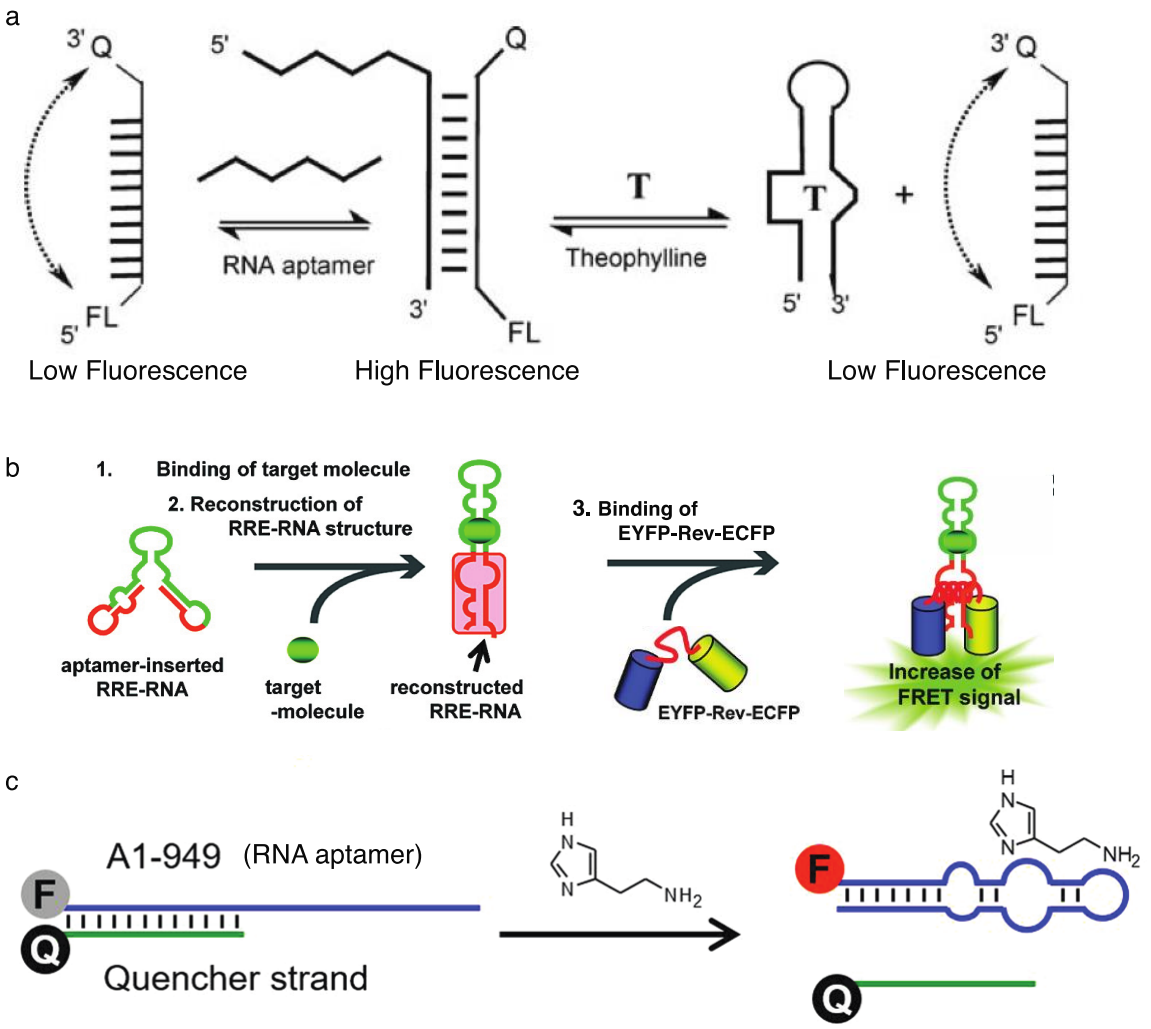

Figure 1.1 Fluorescent-based RNA aptasensors.

(a) Simple theophylline aptasensor. ssDNA is labeled with fluorophore (FL) and quencher (Q).
(b) FRET-based aptasensor for theophylline. Target molecule in green is theophylline.
(c) Aptasensor for detecting histamine. RNA aptamer (A1-949) is labeled with fluorophore (F) and ssDNA (in green) is labeled with quencher (Q). In presence of histamine, quencher strand is displaced and resulting in an increased fluorescence.

1.3 Fluorogenic RNA Aptamers as Biosensor for Nucleic Acids Detection.

Fluorogenic RNA aptamers are RNA aptamers that generate fluorescence upon binding of their otherwise non-fluorescent fluorogen ligands. As a result, these systems represent promising tools for signal transduction and readout in cell-free biosensors. Spinach, an RNA-fluorogen complex that mimics the green fluorescent protein, was identified by performing column-based systematic evolution of ligands by SELEX in 2011 (Fig. 1.2a)[20]. It has been used as a tag for

messenger RNA (mRNA), and has also been adapted for use in protein-free biosensors for detection of proteins and small molecules[21-25].

Current methods for sensing nucleic acids using fluorogenic aptamers can be grouped into three main categories that employ (1) destabilization of the fluorogen-binding site, (2) misfolding of the aptamer sequence, and (3) assembly of split aptamer halves. These general methods have all been implemented using the Spinach aptamer and can be used for in vitro detection and, in some cases, live cell imaging. In systems that destabilize the fluorogen-binding site (Fig. 1.2b), one of the stem regions of an aptamer is disrupted, and its sequence is extended at both ends with those complementary to the target molecule. When the target sequence is present, it hybridizes with the fluorogenic sensor stabilizing the aptamer fold and restoring aptamer fluorescence. This approach has been employed using a modified version of the Spinach aptamer for detection of mRNA and noncoding RNA (e.g., microRNA, small interfering RNA)[26,27]. For the second class of sensors (Fig. 1.2c), the sequence of the aptamer is combined with additional sequences that create strong secondary structures to cause the aptamer to misfold and prevent fluorescence. Upon binding of the target DNA or RNA sequence, a strand displacement reaction occurs causing the aptamer to refold into its active conformation for binding to the fluorogen[28-31]. Sensors of this kind have been used with the Spinach aptamer for diagnostic applications[28,31] and in catalytic RNA amplifier circuits[29]. Lastly, there are binary probes that comprise two halves of aptamer sensors that are unable to hybridize except in the presence of the target DNA or RNA (Fig. 1.2d). Such a split aptamer probe for Spinach was reported by Kikuchi and Kolpashchikov in the sensing of a fragment of the inhA gene from Mycobacterium tuberculosis[32]. They found that the split aptamer design resulted in very low sensor leakage, with only a single base mismatched target producing detectable background fluorescence.

Here, the Spinach aptamer has been used to illustrate the potential of aptamer-based cell-free biosensing, but these concepts can be extended to any other fluorogenic aptamer such as the malachite green and sulforhodamine B binding aptamers, Mango, Corn, Broccoli, and Red Broccoli[30,33-37]. These aptamers can also be combined to enable multiplexed detection.

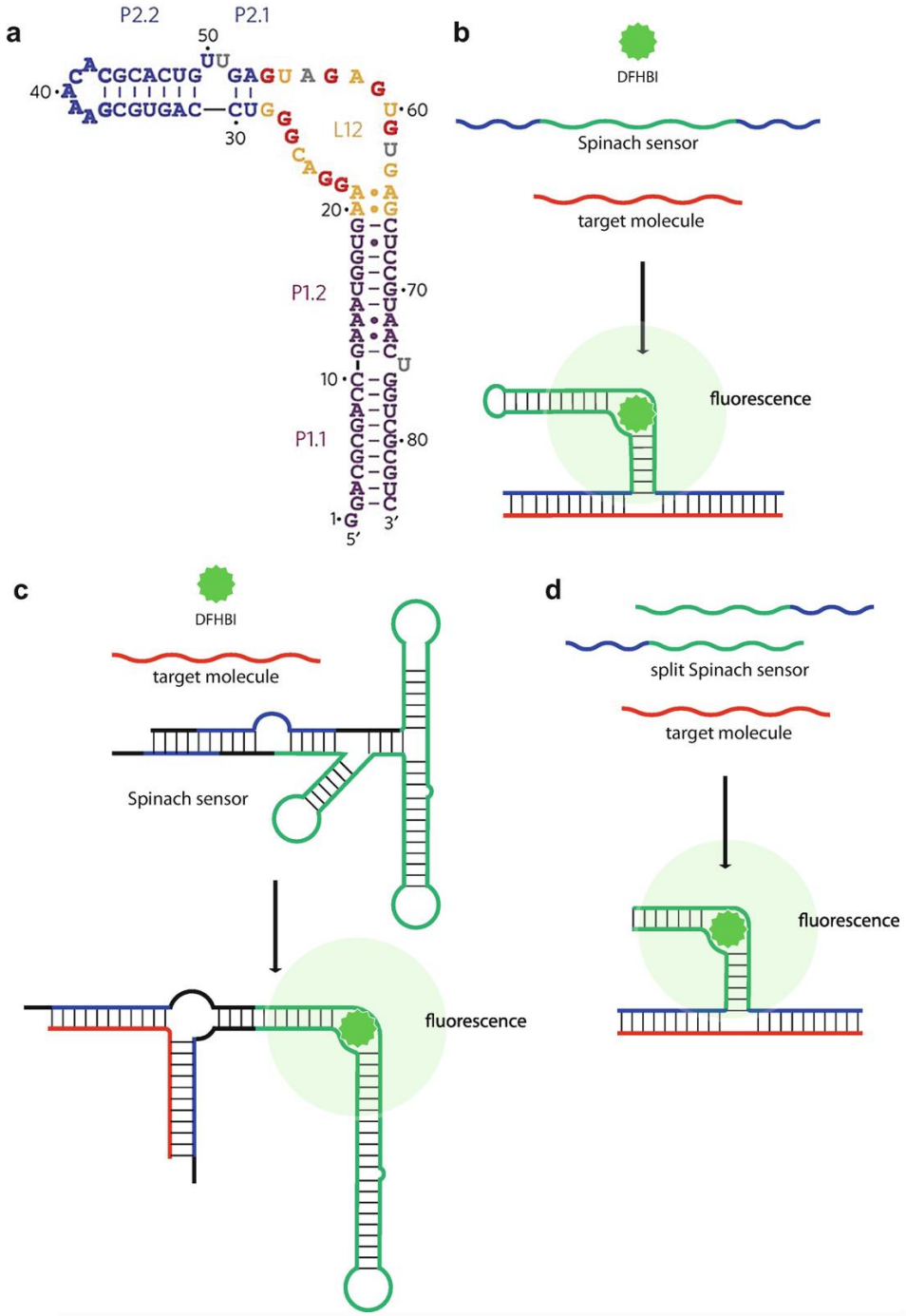

Figure 1.2 Structures of the Spinach-DFHBI complex and Spinach-based sensor designs. (**a**) Sequence and secondary structure of Spinach-DFHBI[38]. (**b**) A Spinach sensor with a destabilized fluorogen-binding site. The sensor remains non-fluorescent until hybridization with a target molecule. (**c**) A Spinach sensor that is triggered by strand displacement based on the design by Huang et al[31].(**d**) A split Spinach nucleic acid sensor. Target molecules are indicated in red, target-binding regions are indicated in blue, and the Spinach aptamer is indicated in green.

1.4 Isothermal Amplification for Detecting Low-Concentration Nucleic Acids.

NASBA was created in 1990 as a way of amplifying single-stranded RNA (ssRNA) in a process that mimics retroviral RNA replication[39]. NASBA's sensitivity is comparable to that of RT-PCR[40], and it can achieve billion-fold RNA amplification in under 2 h at 41 °C. In addition to two primers, the system uses three enzymes: a reverse transcriptase, an RNase H, and a DNA-dependent RNA polymerase (Fig. 1.3). An initial heating step at 65 °C is occasionally performed to deal with the secondary structure of the target RNA[39], but this is not always necessary[41]. The reaction begins with the hybridization of the reverse primer and the target RNA. The reverse transcriptase forms the complementary DNA using the target RNA as template. RNase H degrades the RNA template from the resulting RNA/DNA duplex leaving the cDNA available for binding of the forward primer. The reverse transcriptase is then used to extend the forward primer, producing a dsDNA product. During the process of converting the target RNA into dsDNA, primers are also used to append a promoter sequence (e.g., T7 promoter sequence) to the amplified DNA. The dsDNA is then used as a template for the DNA-dependent RNA polymerase (e.g., T7 RNA polymerase) to create additional copies of the target RNA or its antisense complement. The newly transcribed RNA serves as template for further amplification.

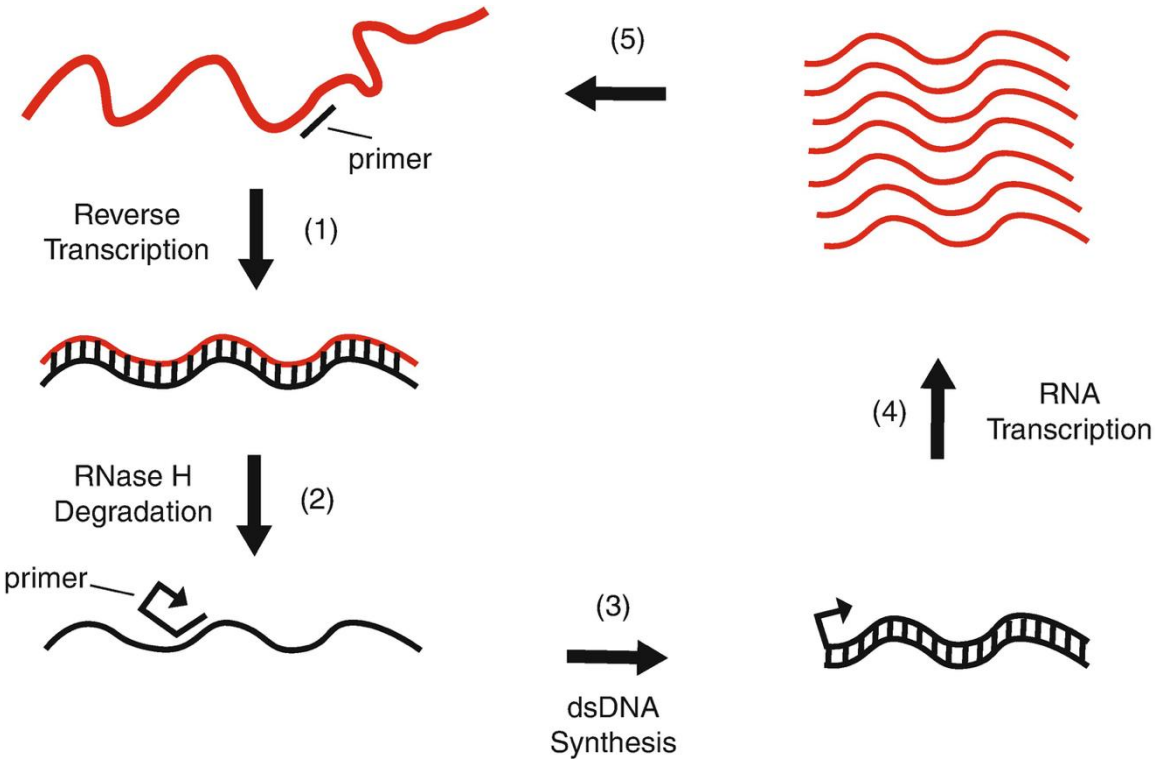

Figure 1.3 Steps involved in the NASBA mechanism[41].
(1) Target RNA is reverse transcribed using the first primer flanking one end of the target sequence. (2) RNase H degrades the template RNA strand. (3) The second primer flanking the other end of the target sequence with an overhang containing the sequence of a promoter is extended on the newly produced complementary DNA strand. (4) The double-stranded product can then be transcribed using a DNA-dependent RNA polymerase to make more RNA copies of the target sequence. (5) The resulting RNA product can be fed back into step 1 to achieve exponential amplification[39].

Loop-mediated isothermal amplification (LAMP) was first introduced by Notomi et al. in 2000 as a way of achieving rapid and highly sequence-specific accumulation of dsDNA[42]. It can produce approximately 10^9 copies[41] of the target in less than one hour. In its simplest form, the method uses four primers. Two inner primers termed FIP and BIP for forward inner primer and backward inner primer, respectively, are used for the bulk of the amplification. Two bumper primers F3 and B3 are used to displace the extension products of FIP and BIP. Together, these four primers recognize six distinct sequences on the template, which is helpful for enforcing sequence specificity of the amplification. A strand-displacing DNA polymerase (e.g., Bst DNA polymerase large fragment) is used for extension of the primers. The inner primers are comprised of two sequences

F1c/F2 and B1c/B2 for FIP and BIP, respectively, as shown in Fig. 1.3. Briefly, hybridization of FIP with the target DNA initiates the amplification process (Fig. 1.4a). The strand-displacing DNA polymerase then extends the FIP and unwinds the target dsDNA (Fig. 1.4b). F3 primer binds to the F3c region on the target leading to displacement of the newly synthesized DNA (Fig. 1.4c–d). This released ssDNA with a loop at the 5' end then serves as template for DNA synthesis primed by BIP and the B3 primer (Fig. 1.4e–g). This process forms a dumbbell-shaped DNA intermediate with seed loops that act as sites of annealing and extension without the need for template denaturation (Fig. 1.4h). The subsequent cycles of elongation and recycling are continued by the inner primer pair, resulting in products with various numbers of stem-looped structures containing alternately inverted repeats of the target sequence[43].

Since positive LAMP reactions become cloudy due to the formation of magnesium pyrophosphate, successful DNA amplification by LAMP can be visually detected with the naked eye. Nonetheless, a number of colorimetric and fluorescence assays have been created for the detection of positive LAMP reactions[44], which further facilitate the use of this method in real-world applications. One drawback of LAMP is its strict requirement for higher temperatures (55–65 °C)[45], which can be contrasted with those of RPA and NASBA (25–42 °C)[40,45,46]. LAMP has been used for highly specific detection of many pathogens including Shiga toxin producing E. coli, Salmonella, and Vibrio parahaemolyticus[47]. Similar to LAMP can also be used to produce a real-time output. For instance, Cao et al. have developed a real-time fluorescence assay for the detection of the common smut of corn, caused by Ustilago maydis. Notably, this work demonstrated a LAMP detection sensitivity 200 times higher than that of conventional PCR[48].

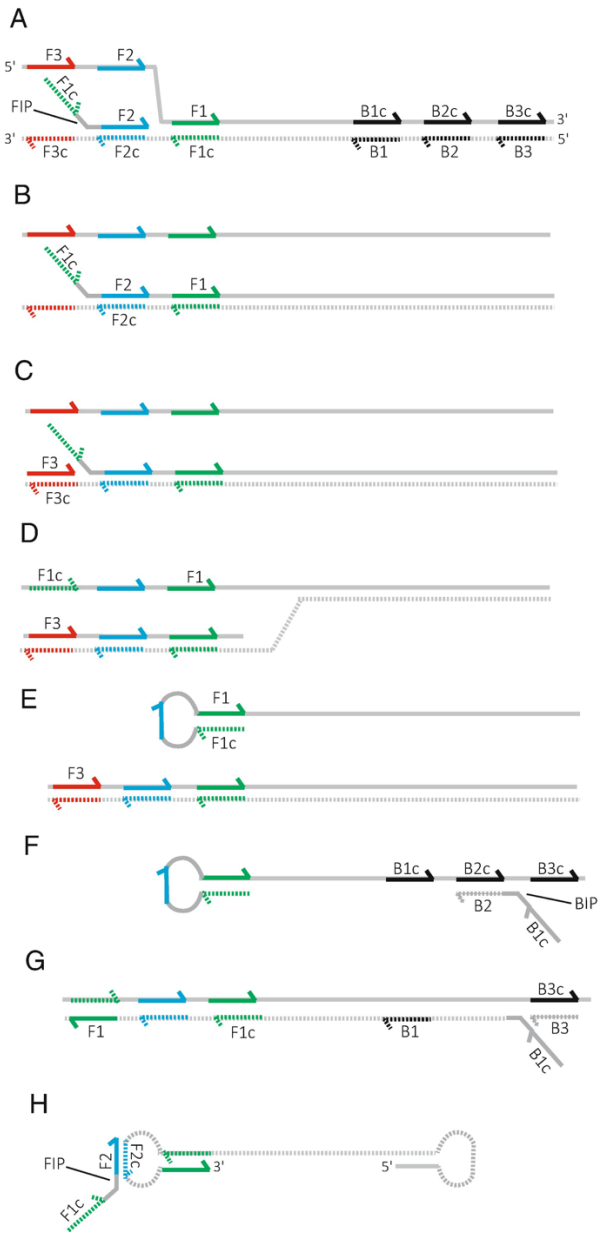

Fig 1.4 Initial steps involved in LAMP. (**a**) FIP (dotted green and solid blue) is designed such that its 5′ end contains an overhang containing F1c (dotted green) and its 3′ end contains the complement to F2c, F2 (solid blue). (**b**) Once annealed to F2c, FIP is extended so that the newly extended strand contains F1c and its complement, F1. (**c**) To release the new strand, the bumper primer F3 (solid red) complementary to F3c is extended by a strand-displacing polymerase. (**d**) The new strand is bumped off the template as the bumper is extended on the original template. (**e**) This results in the release of the newly extended strand that has a section, F1c, self-complementary to its inner sequence, F1. (**f**) A complementary strand is then produced from the inner primer, BIP, which anneals at the other end. (**g**) This complementary strand is bumped off using the second bumper, B3, and the strand-displacing polymerase. (**h**) The resulting new loop

generated at the opposite end can now anneal to the first inner primer, FIP; as the process continues, more loops can act as annealing sites for the inner primers, FIP and BIP. Further extension and loop formation lead to the accumulation of a large number of concatemers under isothermal conditions[42].

In 2006, Piepenburg et al. reported the recombinase polymerase amplification (RPA) method, which amplifies target DNA at 37 °C in 20 min or less with the detection limit as low as a single target copy[46,49,50]. The method can be used to generate double- or single-stranded DNA from RNA or DNA templates. RPA takes advantage of recombinase proteins (e.g., UvsX) which bind to primers in the presence of ATP, forming a nucleoprotein complex. In its active form, the complex interrogates the template strand to find a homologous sequence. This leads to strand invasion by the primer at the cognate site. Primers can then be extended by a strand-displacing polymerase (e.g., Bsu DNA polymerase), providing additional templates for the process. The recombinase-based nucleoprotein complex actively hydrolyses ATP, which results in its disassembly; thus, helper proteins (e.g., UvsY) and crowding agents are used to shift the equilibrium in favor of recombinase loading. To help with primer annealing, single-strand DNA-binding proteins are used to stabilize the displaced strand and to prevent primer ejection by branch migration[46] (Fig. 1.5). Although both LAMP and RPA were first developed for DNA amplification, both methods can be used in concert with a reverse transcriptase for amplification of RNA. RPA tends to be quite fast; in one demonstration, real-time detection of norovirus genomic RNA from human stool samples was accomplished using fluorescent probes in as little as 6 min[51].

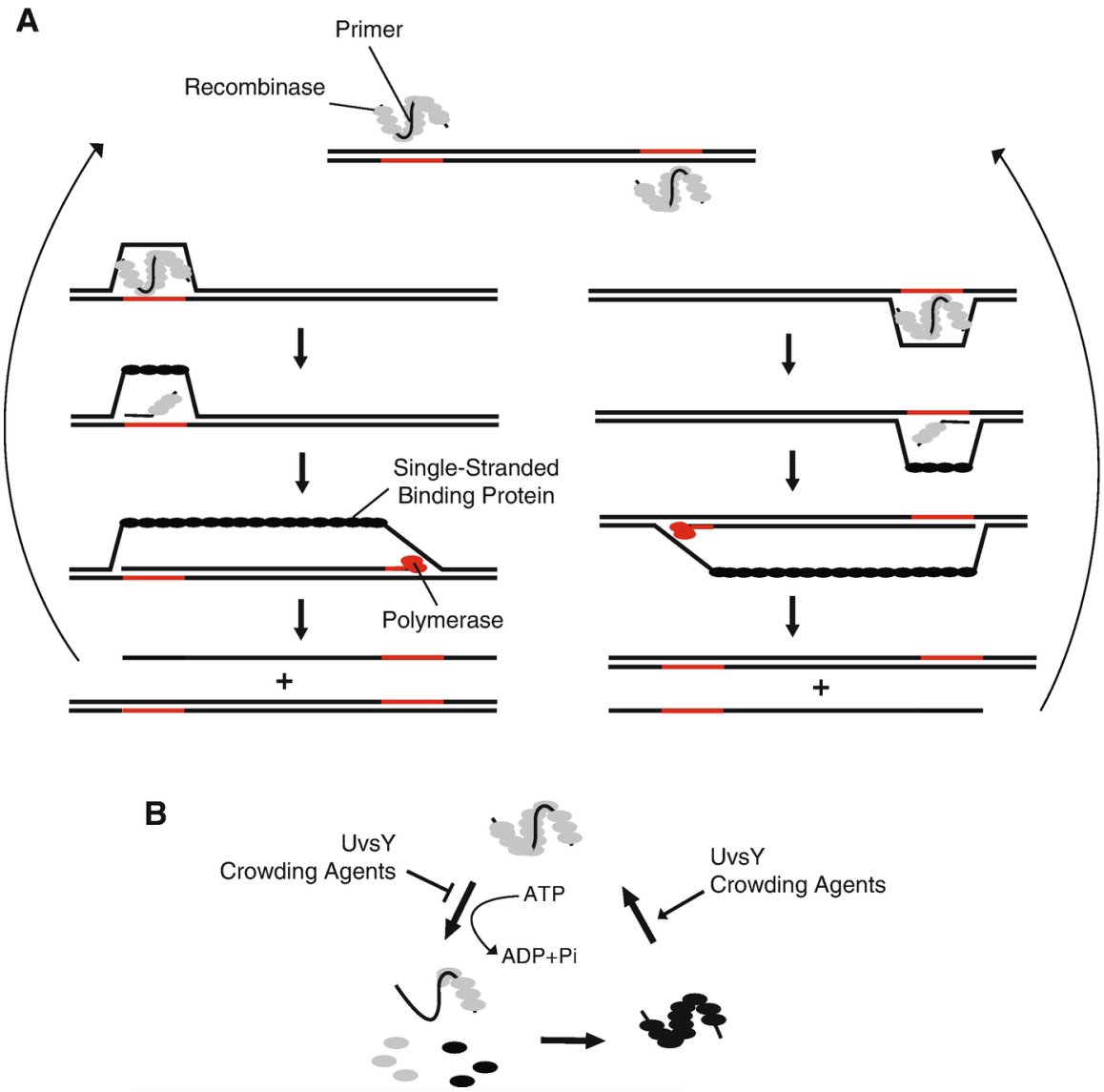

Figure 1.5 The original mechanism developed for RPA.
(**a**) UvsX recombinase forms a nucleoprotein complex with each primer. The complex scans template DNA for a complementary sequence. The displaced strand is bound by the single-strand DNA-binding protein Gp32. Primers are then extended using Bsu polymerase. The resulting two complementary amplicons are fed back into the mechanism to achieve exponential amplification. (**b**) UvsX binds to oligonucleotides in the presence of ATP to form a nucleoprotein complex. Upon hydrolysis of ATP, the complex disassembles and Gp32 replaces UvsX. The helper protein UvsY and the crowding agent Carbowax shift the equilibrium in favor of recombinase [re]loading[46].

1.5 Reference

1 Ellington, A. D. & Szostak, J. W. In vitro selection of RNA molecules that bind specific ligands. *Nature* **346**, 818-822, doi:10.1038/346818a0 (1990).

2 Tuerk, C. & Gold, L. Systematic evolution of ligands by exponential enrichment: RNA ligands to bacteriophage T4 DNA polymerase. *Science* **249**, 505-510, doi:10.1126/science.2200121 (1990).

3 Nutiu, R. & Li, Y. In vitro selection of structure-switching signaling aptamers. *Angew Chem Int Ed Engl* **44**, 1061-1065, doi:10.1002/anie.200461848 (2005).

4 Chang, Y. C. *et al.* Identification and characterization of oligonucleotides that inhibit Toll-like receptor 2-associated immune responses. *Faseb j* **23**, 3078-3088, doi:10.1096/fj.09-129312 (2009).

5 Sefah, K., Shangguan, D., Xiong, X., O'Donoghue, M. B. & Tan, W. Development of DNA aptamers using Cell-SELEX. *Nat Protoc* **5**, 1169-1185, doi:10.1038/nprot.2010.66 (2010).

6 Cheng, C., Chen, Y. H., Lennox, K. A., Behlke, M. A. & Davidson, B. L. In vivo SELEX for Identification of Brain-penetrating Aptamers. *Mol Ther Nucleic Acids* **2**, e67, doi:10.1038/mtna.2012.59 (2013).

7 Fukuda, K. *et al.* Specific RNA aptamers to NS3 protease domain of hepatitis C virus. *Nucleic Acids Symp Ser*, 237-238 (1997).

8 Kumar, P. K. *et al.* Isolation of RNA aptamers specific to the NS3 protein of hepatitis C virus from a pool of completely random RNA. *Virology* **237**, 270-282, doi:10.1006/viro.1997.8773 (1997).

9 Gopinath, S. C., Kawasaki, K. & Kumar, P. K. Selection of RNA-aptamer against human influenza B virus. *Nucleic Acids Symp Ser (Oxf)*, 85-86, doi:10.1093/nass/49.1.85 (2005).

10 Jang, K. J., Lee, N. R., Yeo, W. S., Jeong, Y. J. & Kim, D. E. Isolation of inhibitory RNA aptamers against severe acute respiratory syndrome (SARS) coronavirus NTPase/Helicase. *Biochem Biophys Res Commun* **366**, 738-744, doi:10.1016/j.bbrc.2007.12.020 (2008).

11 Barfod, A., Persson, T. & Lindh, J. In vitro selection of RNA aptamers against a conserved region of the Plasmodium falciparum erythrocyte membrane protein 1. *Parasitol Res* **105**, 1557-1566, doi:10.1007/s00436-009-1583-x (2009).

12 Homann, M. & Göringer, H. U. Uptake and intracellular transport of RNA aptamers in African trypanosomes suggest therapeutic "piggy-back" approach. *Bioorg Med Chem* **9**, 2571-2580, doi:10.1016/s0968-0896(01)00032-3 (2001).

13 Nagarkatti, R., de Araujo, F. F., Gupta, C. & Debrabant, A. Aptamer based, non-PCR, non-serological detection of Chagas disease biomarkers in Trypanosoma cruzi infected mice. *PLoS Negl Trop Dis* **8**, e2650, doi:10.1371/journal.pntd.0002650 (2014).

14 Pan, Q. *et al.* Novel RNA aptamers targeting gastrointestinal cancer biomarkers CEA, CA50 and CA72-4 with superior affinity and specificity. *PLoS One* **13**, e0198980, doi:10.1371/journal.pone.0198980 (2018).

15 Rankin, C. J., Fuller, E. N., Hamor, K. H., Gabarra, S. A. & Shields, T. P. A Simple Fluorescent Biosensor for Theophylline Based on its RNA Aptamer. *Nucleosides, Nucleotides & Nucleic Acids* **25**, 1407-1424, doi:10.1080/15257770600919084 (2006).

16 Endoh, T. *et al.* Detection of Bioactive Small Molecules by Fluorescent Resonance Energy Transfer (FRET) in RNA−Protein Conjugates. *Bioconjugate Chemistry* **20**, 2242-2246, doi:10.1021/bc9002184 (2009).

17 Dwidar, M. & Yokobayashi, Y. Development of a histamine aptasensor for food safety monitoring. *Scientific Reports* **9**, 16659, doi:10.1038/s41598-019-52876-1 (2019).

18 Ling, K. *et al.* A self-assembling RNA aptamer-based nanoparticle sensor for fluorometric detection of Neomycin B in milk. *Anal Bioanal Chem* **408**, 3593-3600, doi:10.1007/s00216-016-9441-z (2016).

19 Jiang, H., Ling, K., Tao, X. & Zhang, Q. Theophylline detection in serum using a self-assembling RNA aptamer-based gold nanoparticle sensor. *Biosensors and Bioelectronics* **70**, 299-303, doi:https://doi.org/10.1016/j.bios.2015.03.054 (2015).

20 Paige, J. S., Wu, K. Y. & Jaffrey, S. R. RNA mimics of green fluorescent protein. *Science* **333**, 642-646, doi:10.1126/science.1207339 (2011).

21 Paige, J. S., Nguyen-Duc, T., Song, W. & Jaffrey, S. R. Fluorescence imaging of cellular metabolites with RNA. *Science* **335**, 1194, doi:10.1126/science.1218298 (2012).

22 Song, W., Strack, R. L. & Jaffrey, S. R. Imaging bacterial protein expression using genetically encoded RNA sensors. *Nat Methods* **10**, 873-875, doi:10.1038/nmeth.2568 (2013).

23 Strack, R. L., Song, W. & Jaffrey, S. R. Using Spinach-based sensors for fluorescence imaging of intracellular metabolites and proteins in living bacteria. *Nat Protoc* **9**, 146-155, doi:10.1038/nprot.2014.001 (2014).

24 You, M., Litke, J. L. & Jaffrey, S. R. Imaging metabolite dynamics in living cells using a Spinach-based riboswitch. *Proc Natl Acad Sci U S A* **112**, E2756-2765, doi:10.1073/pnas.1504354112 (2015).

25 Svensen, N. & Jaffrey, S. R. Fluorescent RNA Aptamers as a Tool to Study RNA-Modifying Enzymes. *Cell Chem Biol* **23**, 415-425, doi:10.1016/j.chembiol.2015.11.018 (2016).

26 Ong, W. Q., Citron, Y. R., Sekine, S. & Huang, B. Live Cell Imaging of Endogenous mRNA Using RNA-Based Fluorescence "Turn-On" Probe. *ACS Chem Biol* **12**, 200-205, doi:10.1021/acschembio.6b00586 (2017).

27 Aw, S. S., Tang, M. X., Teo, Y. N. & Cohen, S. M. A conformation-induced fluorescence method for microRNA detection. *Nucleic Acids Res* **44**, e92, doi:10.1093/nar/gkw108 (2016).

28 Bhadra, S. & Ellington, A. D. A Spinach molecular beacon triggered by strand displacement. *RNA* **20**, 1183-1194, doi:10.1261/rna.045047.114 (2014).

29 Akter, F. & Yokobayashi, Y. RNA signal amplifier circuit with integrated fluorescence output. *ACS Synth Biol* **4**, 655-658, doi:10.1021/sb500314r (2015).

30 Ying, Z. M., Wu, Z., Tu, B., Tan, W. & Jiang, J. H. Genetically Encoded Fluorescent RNA Sensor for Ratiometric Imaging of MicroRNA in Living Tumor Cells. *J Am Chem Soc* **139**, 9779-9782, doi:10.1021/jacs.7b04527 (2017).

31 Huang, K. *et al.* FASTmiR: an RNA-based sensor for in vitro quantification and live-cell localization of small RNAs. *Nucleic Acids Res.* **45**, doi:10.1093/nar/gkx504 (2017).

32 Kikuchi, N. & Kolpashchikov, D. M. Split Spinach Aptamer for Highly Selective Recognition of DNA and RNA at Ambient Temperatures. *Chembiochem* **17**, 1589-1592, doi:10.1002/cbic.201600323 (2016).

33 Song, W. *et al.* Imaging RNA polymerase III transcription using a photostable RNA-fluorophore complex. *Nat Chem Biol* **13**, 1187-1194, doi:10.1038/nchembio.2477 (2017).

34 Alam, K. K., Tawiah, K. D., Lichte, M. F., Porciani, D. & Burke, D. H. A Fluorescent Split Aptamer for Visualizing RNA-RNA Assembly In Vivo. *ACS Synth Biol* **6**, 1710-1721, doi:10.1021/acssynbio.7b00059 (2017).

35 Kolpashchikov, D. M. Binary Malachite Green Aptamer for Fluorescent Detection of Nucleic Acids. *Journal of the American Chemical Society* **127**, 12442-12443, doi:10.1021/ja0529788 (2005).

36 Dolgosheina, E. V. *et al.* RNA mango aptamer-fluorophore: a bright, high-affinity complex for RNA labeling and tracking. *ACS Chem Biol* **9**, 2412-2420, doi:10.1021/cb500499x (2014).

37 Sato, S. *et al.* Live-Cell Imaging of Endogenous mRNAs with a Small Molecule. *Angew. Chem.-Int. Edit.* **54**, 1855-1858, doi:10.1002/anie.201410339 (2015).

38 Huang, H. *et al.* A G-quadruplex-containing RNA activates fluorescence in a GFP-like fluorophore. *Nat. Chem. Biol.* **10**, 686-U128, doi:10.1038/nchembio.1561 (2014).

39 Guatelli, J. C. *et al.* Isothermal, in vitro amplification of nucleic acids by a multienzyme reaction modeled after retroviral replication. *Proc Natl Acad Sci U S A* **87**, 1874-1878, doi:10.1073/pnas.87.5.1874 (1990).

40 Burchill, S. A., Perebolte, L., Johnston, C., Top, B. & Selby, P. Comparison of the RNA-amplification based methods RT-PCR and NASBA for the detection of circulating tumour cells. *Br J Cancer* **86**, 102-109, doi:10.1038/sj.bjc.6600014 (2002).

41 Pardee, K. *et al.* Rapid, Low-Cost Detection of Zika Virus Using Programmable Biomolecular Components. *Cell* **165**, 1255-1266, (2016).

42 Notomi, T. *et al.* Loop-mediated isothermal amplification of DNA. *Nucleic Acids Res.* **28**, 7, doi:10.1093/nar/28.12.e63 (2000).

43 Zhao, Y., Chen, F., Li, Q., Wang, L. & Fan, C. Isothermal Amplification of Nucleic Acids. *Chem Rev* **115**, 12491-12545, doi:10.1021/acs.chemrev.5b00428 (2015).

44 Goto, M., Honda, E., Ogura, A., Nomoto, A. & Hanaki, K. Colorimetric detection of loop-mediated isothermal amplification reaction by using hydroxy naphthol blue. *Biotechniques* **46**, 167-172, doi:10.2144/000113072 (2009).

45 Xing, W. *et al.* Field evaluation of a recombinase polymerase amplification assay for the diagnosis of Schistosoma japonicum infection in Hunan province of China. *BMC Infect Dis* **17**, 164, doi:10.1186/s12879-017-2182-6 (2017).

46 Piepenburg, O., Williams, C. H., Stemple, D. L. & Armes, N. A. DNA Detection Using Recombination Proteins. *PLOS Biology* **4**, e204, doi:10.1371/journal.pbio.0040204 (2006).

47 Li, Y., Fan, P., Zhou, S. & Zhang, L. Loop-mediated isothermal amplification (LAMP): A novel rapid detection platform for pathogens. *Microb Pathog* **107**, 54-61, doi:10.1016/j.micpath.2017.03.016 (2017).

48 Cao, Y. *et al.* Development of a real-time fluorescence loop-mediated isothermal amplification assay for rapid and quantitative detection of Ustilago maydis. *Sci Rep* **7**, 13394, doi:10.1038/s41598-017-13881-4 (2017).

49 Oriero, E. C., Jacobs, J., Van Geertruyden, J. P., Nwakanma, D. & D'Alessandro, U. Molecular-based isothermal tests for field diagnosis of malaria and their potential contribution to malaria elimination. *J Antimicrob Chemother* **70**, 2-13, doi:10.1093/jac/dku343 (2015).

50 Lobato, I. M. & O'Sullivan, C. K. Recombinase polymerase amplification: Basics, applications and recent advances. *Trends Analyt Chem* **98**, 19-35, doi:10.1016/j.trac.2017.10.015 (2018).

51 Moore, M. D. & Jaykus, L. A. Development of a Recombinase Polymerase Amplification Assay for Detection of Epidemic Human Noroviruses. *Sci Rep* **7**, 40244, doi:10.1038/srep40244 (2017).

CHAPTER 2

BROCCOLI-BASED APTASENSORS: HIGH-PERFORMANCE FLUOROGENIC RNA SENSORS WITHOUT SEQUENCE CONSTRAINTS

2.1 Introduction

RNA aptamers are defined as RNA oligonucleotides that bind to a specific target with high affinity and specificity[1,2]. RNA aptamers that are able to specifically interact with a fluorogen to form a fluorescent complex are known as fluorogenic RNA aptamers. In 2011, Jaffrey and co-workersr[20] reported the first GFP-derived fluorogens and their cognate RNA aptamer Spinach. Soon thereafter, the Broccoli[52] aptamer was selected by the same group demonstrating increased fluorescence, shortened aptamer length, and improved thermostability. The Broccoli fluorophore, (*Z*)-4-(3,5-difluoro-4-hydroxybenzylidene)-2-methyl-1-(2,2,2-trifluoroethyl)-1*H* imidazol-5(4*H*)-one) (DFHBI-1T), is a structural mimic of the GFP fluorophore, 4-hydroxybenzylidene-imidazolinone (HBI). These fluorogenic RNA aptamers have been used as tags for *in vivo* mRNA imaging and in biosensors for detecting proteins and small molecules[21-25]. Challenges for adaptation of fluorogenic aptamers for RNA sensing including poor signal-to-noise ratios and sequence constraints of target RNA[26,28,37,53].

In this study, we established three designs for Broccoli-based aptasensor capable of detecting a variety of different target RNA sequences. All the designs form an active Broccoli-DFHBI-1T complex only in the presence of the cognate target RNA. The first design employs a linear-linear interaction between a single-stranded toehold region upstream of the stem-loop containing a repressed Broccoli and a single-stranded target RNA, and we refer to it as toehold-initiated aptasensor. The binding between target RNA and second type of aptasensor is initiated by a loop-linear interaction occurred from the binding between the target RNA and the loop portion of the stem-loop aptasensor. For the final aptasensor design, the Broccoli aptamer was split with half of it sequestered in a stem-loop structure of the sensor. Upon binding with the cognate target RNA, the two halves of the Broccoli will reunite and activate fluorescence. Toehold-initiated Broccoli-based RNA aptasensors provided lowest signal leakage and most robust fluorescence in

presence of the RNA target. Testing of the toehold-initiated aptasensors has demonstrated that these systems can provide ON/OFF ratios over 100-fold.

2.2 Materials and Methods

2.2.1 DNA template preparation

All DNA oligonucleotides were designed using the NUPACK software package as briefly described in the Results section and purchased from Integrated DNA Technologies. DNA fragments were assembled and amplified via PCR using Phusion High-Fidelity PCR Master Mix with HF Buffer (NEB, M0531L). PCR product of the aptasensor was purified by using MinElute PCR Purification Kit (Qiagen, 28006).

2.2.2 RNA synthesis

Aptasensor RNA was transcribed *in vitro* using AmpliScribe™ T7-Flash™ Transcription Kits (Lucigen, ASF3507) from 0.1 μM of the DNA template at 37 °C for 2 hours. Target RNA was directly synthesized from PCR amplified product and was purified using RNA Clean & Concentrator™-25 (Zymo Research, R1017). For quantified of RNAs, DNase I (Lucigen, ASF3507) was used to remove DNA template for the termination of the transcription.

2.2.3 Plate Reader Measurements

A BioTek Synergy H1 Multi-Mode Reader was used for all plate reader measurements. 96 and 384 well plates were used for sensor screening and small-scale measurements, respectively. Before each measurement, samples were shaken linearly for 30 seconds to ensure proper mixing. The plate reader was preheated, and the measurements were all taken at 37°C unless otherwise indicated. Approximately 0.5 μM or 2 μL of aptasensor RNA, 2.5 μM of purified target RNA were added to the assay plate along with 20 μM of DFHBI-1T (Lucerna, 410) for the initial testing, and 4 μM of DFHBI-1T for the screening for pathogen specific aptasensors. DFHBI-1T buffer is consisted of 40 mM HEPES pH 7.4, 100 mM KCl, 1 mM MgCl2 and 4μM / 20μM DFHBI-1T.

2.3 Results and Discussion

2.3.1 Determining the effect of sequence changes to Broccoli fluorescent output.

The secondary structures of the Broccoli aptamers were shown in Fig. 2.1a. We termed the Broccoli aptamer on the top the standard Broccoli, as it is in the configuration first reported by Filonov et al[52]. We termed the Broccoli aptamer on bottom the rotated Broccoli, as it is a circular permutation of the original aptamer. We hypothesized that the stem at the terminals is essential to ensure proper folding of the aptamers[54]. In order to determine if the aptamer could be incorporated into aptasensors capable of detecting different sequences, we initially studied the effect of sequence changes in the terminal stems of the standard and rotated forms of the Broccoli aptamer.

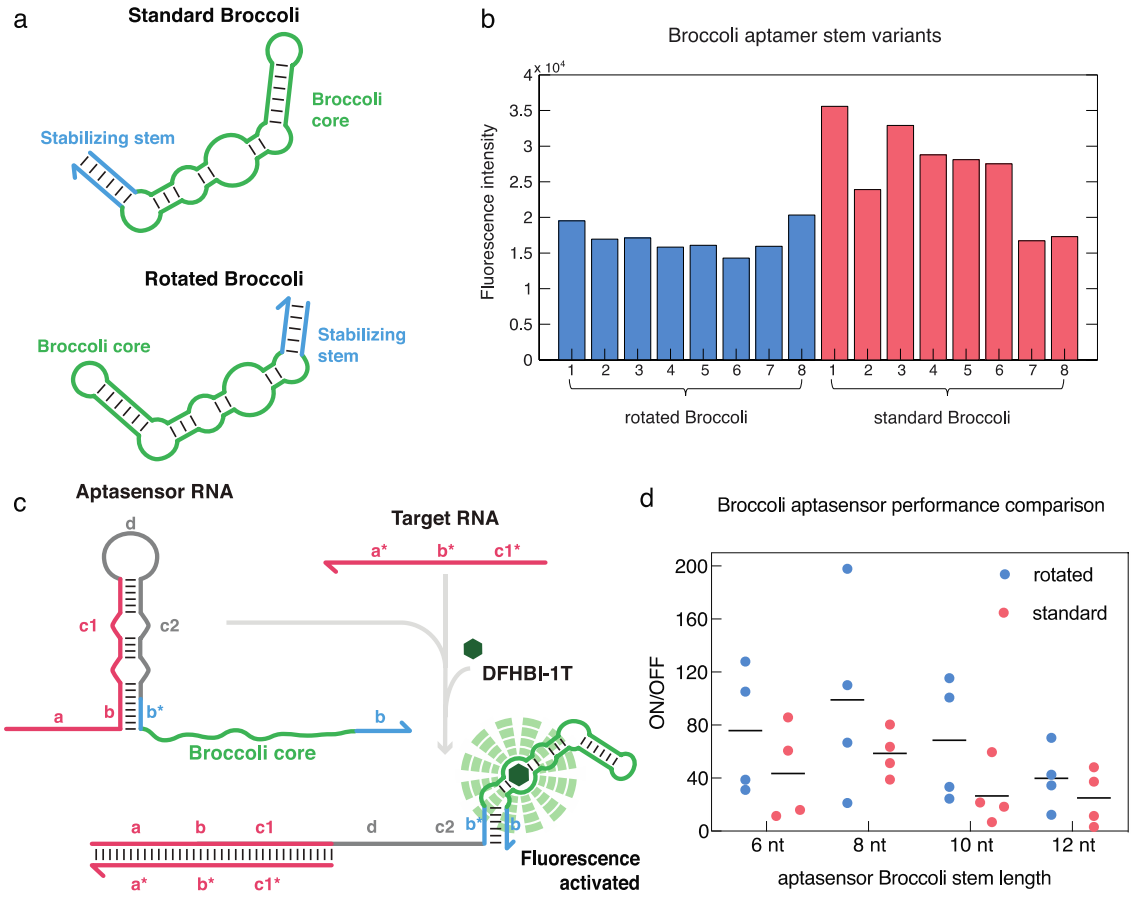

Figure 2.1 Broccoli aptamer and the toehold-initiated Broccoli-based aptasensor.

(a) Structures of the standard and rotated Broccoli aptamer. The standard Broccoli is the original Broccoli, and the rotated Broccoli is the circular-permutated Broccoli.

(b) The performance of the Broccoli aptamer with various stem sequences. Eight different stem sequences were tested for both standard and rotated Broccoli.

(c) Design of the toehold-initiated Broccoli-based aptasensor. Hairpin structure sequestering the stabilizing stem of the Broccoli represses the formation of the Broccoli/DFHBI-1T complex. The a* domain in the target RNA binds to a complementary, single-stranded toehold a domain in the sensor RNA, initiating a branch migration that opens the hairpin stem. Newly freed b* domain binds to the downstream b domain, enabling the formation of the Broccoli-DFHBI-1T complex.

(d) Evaluation of the **b** domain (Broccoli stem) length of the aptasensors. Data represent mean ON/OFF of 4 aptasensors with the same b domain length. ON/OFF is the ratio of the mean fluorescence for the sensor alone and sensor plus target RNA.

For successful inclusion in sensor designs, it is essential to have an aptamer stem that is insensitive to changes in its sequence. Thus, we made changes to the stem sequences of both standard and rotated forms of Broccoli and measured fluorescent intensities of the resulting Broccoli-DFHBI-1T complexes. We tested 8 stem variants for both standard and rotated Broccoli aptamers. Although standard Broccoli aptamers provided overall higher fluorescence, rotated Broccoli aptamers were less sensitive to changes in stem sequence which suggests more reliable integration with sensors for detection of arbitrary target RNAs (Fig. 2.1b). In addition, the standard Broccoli aptamers possess a slightly longer stem than the rotated broccoli aptamers, which likely improved folding and increased their fluorescence compared to the rotated variants.

2.3.2 Design of toehold-initiated Broccoli-based aptasensor.

The toehold-initiated Broccoli-based RNA aptasensor employs a switch RNA with a 5′ toehold (domain a), a 15-nt region that initiates the interaction with the target RNA (Fig. 2.1c). The 15-nt toehold domain is followed by a 20-nt stem and 8-nt loop structure with two 1-nt bulges in the **c/c*** domains, where the "*" symbol denotes a complementary sequence. The Broccoli aptamer core, which lacks the stabilizing stem, is positioned downstream of the RNA sensing element. The adjacent **b/b*** domains complete the Broccoli aptamer and are responsible for stabilizing of the correct conformation of the Broccoli aptamer upon target RNA binding. In absence of the target RNA, Broccoli-based RNA sensor will not be stably folded as the **b*** domain is sequestered within the stem, thus the system is non-fluorescent. In the presence of the target RNA, the **b*** domain will be released from the stem-loop structure of the sensor and it will hybridize with the downstream **b**

domain. As result, Broccoli aptamer is securely folded, and activates the fluorescence of the fluorophore DFHBI-1T.

We increased the length of **b** domain (from 6 to 12 nts with 2-nt increments) to increase the ON-state signal making the aptasensor-DFHBI-1T complex more stable. We tested sensors with conserved or arbitrary **b** domains for both versions of Broccoli aptamers. We observed that 16 out of the 32 Broccoli-based aptasensors exhibited ON/OFF ratios over 40, and six provided ON/OFF ratios over 100 (Fig. 2.1d). Aptasensors with rotated Broccoli had overall higher ON/OFF ratios compared with ones with standard Broccoli. In a comparison of aptasensors with a 12-nt **b** domain to the ones with a **b** domain length from 6 to 10 nts, the latter offered higher mean ON/OFF. These results revealed that Broccoli-based aptasensors with arbitrary **b** domain sequences can provide performance as good or better than those employing the conserved aptamer stem sequences.

2.3.3 Design of loop-initiated Broccoli-based aptasensor.

Compared to the toehold-initiated Broccoli-based aptasensor, the loop-initiated one (Fig. 2.2a) has a larger loop and a longer stem. The size of the loop in this stem-loop structure upstream of the rotated Broccoli core is increased from 8 to 21-nts, and the size of the stem is increased from 20 to 27-nts. The target RNA binds to the exposed bases in the sensor RNA loop (**b** domain) initiating the RNA-RNA interaction, and proceeds to hybridize with the bases in the stem (**a** domain). The formation of the target-sensor RNA duplex causes the remaining base pairs in the stem to unwind. The newly released **c** domain, the stabilizing stem of the Broccoli, binds to its complementary sequence **c*** downstream of the Broccoli core, and activates fluorescence of the complex in presence of the DFHBI-1T. We designed 24 loop-initiated aptasensors via NUPACK with half of the target RNA hybridizing to the left side of the stem, and the other half hybridizing to the right side (Fig. 2.2b). We also varied the length of the stabilizing stem (**c** domain) ranging from 6-nt to 12-nt. The aptasensors with their cognate target RNA binding to the left (Fig. 2.2c) had a overall higher ON/OFF than the other half of the aptasensors (Fig. 2.2d). Two thirds of the

aptasensors (left) provided ON/OFF ratios over 5-fold and in which three had ON/OFF over 15-fold. The leakage was higher and the brightness or the ON-state fluorescence intensity was lower in contrast to the toehold-initiated sensors (Fig. 2.2e,f).

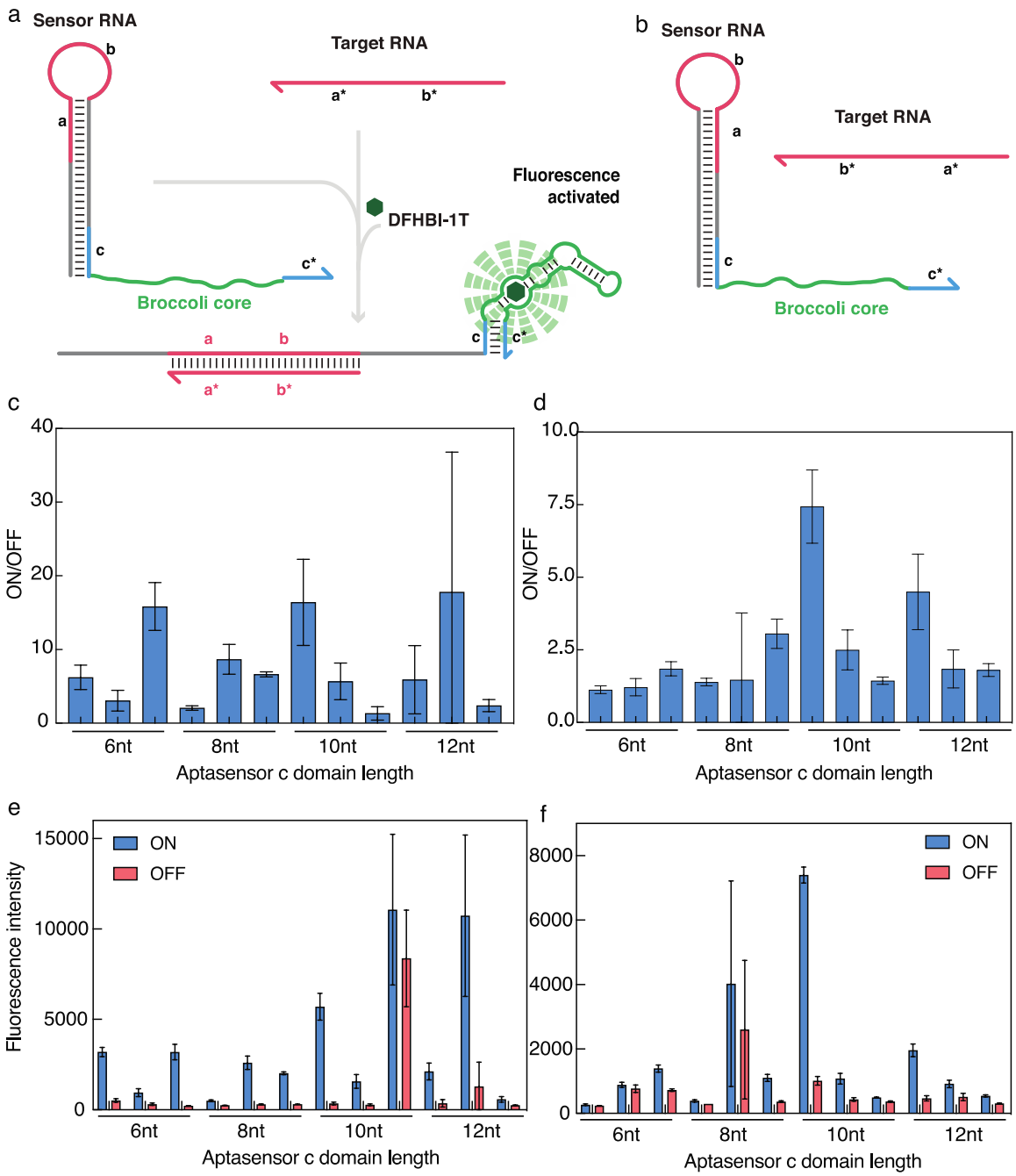

Figure 2.2 Loop-initiated Broccoli-based aptasensors.

(a) Schematic of loop-initiated aptasensors. The hybridization of the target RNA and the sensor RNA disrupts the remaining base pairs in the sensor RNA, and exposes Broccoli stem (**c** domain).

(b) Target RNA binding to the loop and the downstream region (right).
(c) ON/OFF ratios for aptasensor with target RNA binding to the loop and the upstream region (left).
(d) ON/OFF ratios for aptasensor with target RNA binding to the loop and the downstream region (right).
(e) ON- and OFF-state fluorescence data for (left)- aptasensors.
(f) ON- and OFF-state fluorescence data for (right)- aptasensors.
The relative errors for the ON- and OFF- states are from the s.d. of n = 3 biological replicates.

2.3.4 Design of unimolecular split Broccoli-based aptasensor.

In our unimolecular split aptasensor design (Fig. 2.3a), we positioned one half of the aptamer at the loop of the sensor (domain **X** = UCUGAGACGGUCGGGUC) and sequestered it from the other half (domain **Y =** UCGAGUAGAGUGUGGGCUCAGA) and removed 4-nt 'UUCG' at the terminal loop (Fig. 2.3a). To compensate for this 4-nt removal, we inserted z and z* domains for better stabilization of the active Broccoli upon hybridization to the target RNA. Upon binding of the target RNA, the stem-loop of the sensor will be gradually disrupted, and the binding of the **c*** domain to the downstream **c** domain will bring into close proximity both halves of the Broccoli aptamer. In turn, this localization of the two halves activates the fluorescence. For the split Broccoli aptasensor designs, we also varied the length of **c**/**c*** domains from six to eight nucleotides. We tested 12 constructs of the aptasensor (Fig. 2.3b), and one aptasensor with seven-nucleotide stabilizing stem provided highest ON/OFF over ten-fold. These unimolecular split aptasensors had the highest signal leakage (Fig 2.3c) when compared with aptasensor for the previous two designs. The correct folded Broccoli conformation of the aptasensor was more favorable with increased **c** domains in absence of the target RNA.

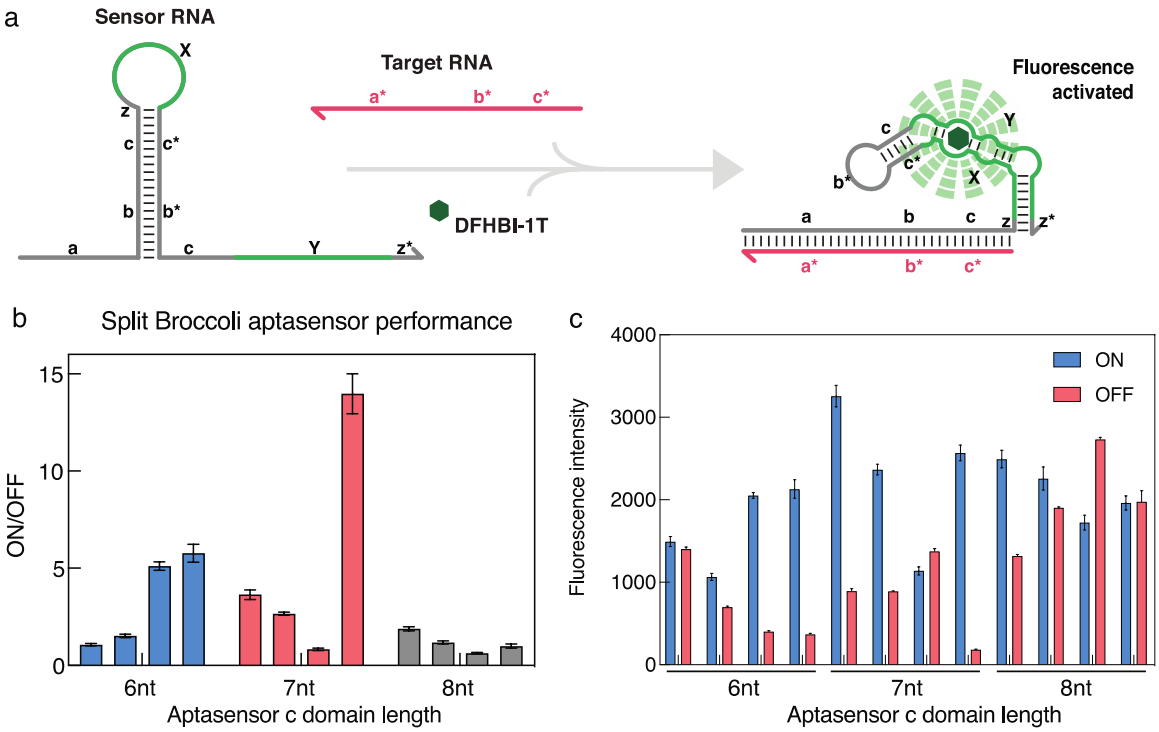

Figure 2.3 Unimolecular split Broccoli aptasensors.

(a) Schematic of unimolecular split Broccoli aptasensors. Target RNA binds to the single-strand toehold region and unwinds the stem of the sensor RNA. Two halves of the Broccoli come together and activate the fluorescence in presence of the DFHBI-1T.

(b) ON/OFF ratios for 12 different unimolecular split Broccoli aptasensors. The relative errors for the ON- and OFF- states are from the s.d. of n = 3 technical replicates.

(c) ON- and OFF-state fluorescence data for unimolecular split Broccoli aptasensors. The relative errors for the ON- and OFF- states are from the s.d. of n = 3 technical replicates.

2.3.5 Targeting toehold-initiated aptasensor to pathogen-related RNAs.

Toehold-initiated aptasensor designs that provided the highest ON/OFF ratios were selected for the subsequent studies for detection pathogen RNA. Aptasensors were designed for each potential binding site along the target RNA in 1-nt increments, leaving flanking regions on the 5' and 3' ends of the target available for primer binding. The resulting Broccoli-based aptasensors were screened for secondary structure and toehold availability using a design algorithm based on NUPACK[55]. We implemented designs using rotated Broccoli and specified **b** domain lengths that ranged from 6 to 10 nt, based on the findings reported in Figure 2.1d. Top six to eight constructs with lowest overall defects for each target were screened experimentally. The screening process

for the pathogen detecting aptasensor is described in Materials and Methods section. Briefly, we combined the individually transcribed sensor RNA with an excess of synthetic target RNA in 4 μM of DFHBI-1T buffer. Using a plate reader, we measured the samples continuously for two hours at 37°C. Background fluorescence from DFHBI-1T alone was not subtracted from either the ON- or OFF-state fluorescence for determination of the ON/OFF ratio.

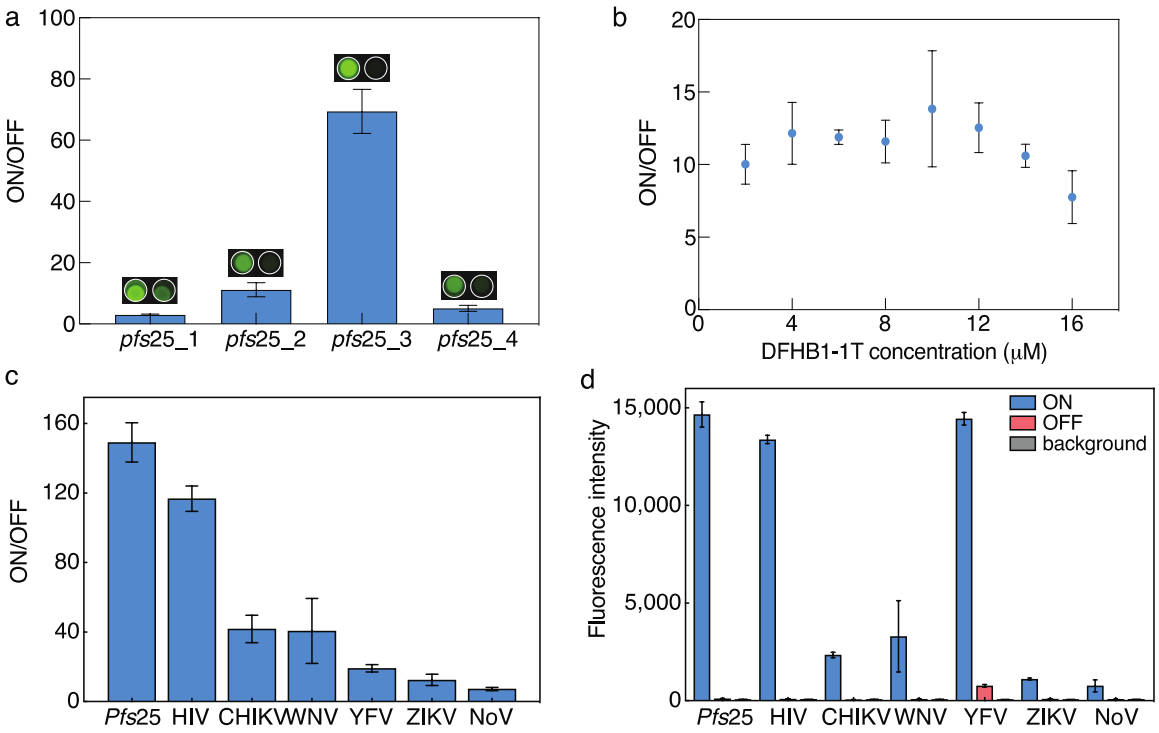

Figure 2.4 Characterization of the toehold-initiated aptasensors for detecting pathogen RNA.

(a) Screening of the Broccoli aptasensors for targeting *pfs*25 gene of malaria. Photographs of fluorescence from the sensors in the presence or absence of the cognate target RNA are shown above the bars. The relative errors are from the s.d. of n = 3 biological replicates.

(b) DFHBI-1T titration experiment with *pfs*25_3 aptasensor and cognate target RNA. The relative errors are from the s.d. of n = 3 technical replicates.

(c) Best performing Broccoli aptasensors targeting RNAs for each pathogen species. Data represent the ON/OFF fluorescence ratio from the sensors in the presence or absence of the cognate target RNA. The relative errors are from the s.d. of n = 3 biological replicates.

(d) Best performing Broccoli aptasensors targeting RNAs for each pathogen species. Data represent mean fluorescence from the sensors in the presence or absence of the cognate target RNA and background fluorescence of DFHBI-1T in absence of RNA. The relative errors are from the s.d. of n = 3 biological replicates.

The first set of sensors was designed for detection of the malaria parasite *Plasmodium falciparum*. In 2018, there were an estimated 228 million cases of malaria infection with an estimated 405,000 deaths from malaria, and children under the age of five accounted for 67% of all malaria deaths worldwide[56]. *Plasmodium falciparum* is the most prevalent malaria parasite causing 99.7% of the estimated malaria infections in African region[56]. We generated 16 aptasensors targeting the sense and antisense sequences of a fragment of gene *pfs25* (surface protein of *P. falciparum*)[57]. The ON/OFF ratio of the first four aptasensors for the sense sequence is shown in Figure 2.4a. Although *pfs*25_1 provided the lowest the ratio of 3.0 among these four aptasensor, one can still distinguish its ON state from its OFF state by eye or a smartphone. To determine the minimum DFHBI-1T we could use for screening the sensors, we chose aptasensor *Pfs*25_3 for DFHBI-1T titration experiments. We incubated 1 μM of sensor and target RNA with DFHBI-1T of various concentrations (Fig. 2.4b), and found out the fluorescence was effectively activated with as low as 4 μM of DFHBI-1T.

To demonstrate the high programmability of our Broccoli-based aptasensor, we generated Broccoli-based RNA sensors targeting more pathogens, including human immunodeficiency viruses (HIV), yellow fever virus (YFV), West Nile virus (WNV), zika virus (ZIKV), Chikungunya virus (CHIKV), and norovirus (NoV). By downloading and aligning hundreds of complete and partial genome sequences from the NCBI database, we identified conserved sequence regions of YFV genome the suitable for isothermal amplification. We selected a 200-nt target sequence that was highly conserved across the genomes for subsequent experiments. Target sequences for the rest of the pathogens were taken from previous reported detection assays [41,58-61]. The best performing aptasensor for each pathogen (Fig. 2.4c) were chosen based on highest fold change in fluorescence intensity with sensors activated by cognate target RNA. All seven aptasensors were activated within 30 min of incubation, with two of them exhibited ON/OFF over 100-fold. We observed that the OFF state of most aptasensors (Fig. 2.4d) provided low leakage compared with output nearly the same as DFHBI-1T background fluorescence.

2.4 Conclusion

We introduced three strategies for the design of Broccoli-based aptasensors enabling detection of target RNA without any sequence constraints: toehold-initiated, loop-initiated and unimolecular split RNA sensor. Toehold-initiated designs had the best performance and were used for developing pathogen-related aptasensors. We demonstrated the broad adaptability and programmability of the aptasensor by targeting seven different pathogen RNAs. Toehold-initiated Broccoli-based aptasensors provided high dynamic range and low signal leakage *in vitro* and could be suitable for applications such as *in vivo* RNA imaging and *in vitro* nucleic acid diagnostics.

2.5 References

1 Ellington, A. D. & Szostak, J. W. In vitro selection of RNA molecules that bind specific ligands. *Nature* **346**, 818-822, doi:10.1038/346818a0 (1990).

2 Tuerk, C. & Gold, L. Systematic evolution of ligands by exponential enrichment: RNA ligands to bacteriophage T4 DNA polymerase. *Science* **249**, 505-510, doi:10.1126/science.2200121 (1990).

3 Paige, J. S., Wu, K. Y. & Jaffrey, S. R. RNA mimics of green fluorescent protein. *Science* **333**, 642-646, doi:10.1126/science.1207339 (2011).

4 Filonov, G. S., Moon, J. D., Svensen, N. & Jaffrey, S. R. Broccoli: Rapid Selection of an RNA Mimic of Green Fluorescent Protein by Fluorescence-Based Selection and Directed Evolution. *Journal of the American Chemical Society* **136**, 16299-16308, doi:10.1021/ja508478x (2014).

5 Paige, J. S., Nguyen-Duc, T., Song, W. & Jaffrey, S. R. Fluorescence imaging of cellular metabolites with RNA. *Science* **335**, 1194, doi:10.1126/science.1218298 (2012).

6 Song, W., Strack, R. L. & Jaffrey, S. R. Imaging bacterial protein expression using genetically encoded RNA sensors. *Nat Methods* **10**, 873-875, doi:10.1038/nmeth.2568 (2013).

7 Strack, R. L., Song, W. & Jaffrey, S. R. Using Spinach-based sensors for fluorescence imaging of intracellular metabolites and proteins in living bacteria. *Nat Protoc* **9**, 146-155, doi:10.1038/nprot.2014.001 (2014).

8 You, M., Litke, J. L. & Jaffrey, S. R. Imaging metabolite dynamics in living cells using a Spinach-based riboswitch. *Proc Natl Acad Sci U S A* **112**, E2756-2765, doi:10.1073/pnas.1504354112 (2015).

9 Svensen, N. & Jaffrey, S. R. Fluorescent RNA Aptamers as a Tool to Study RNA-Modifying Enzymes. *Cell Chem Biol* **23**, 415-425, doi:10.1016/j.chembiol.2015.11.018 (2016).

10 Sato, S. *et al.* Live-Cell Imaging of Endogenous mRNAs with a Small Molecule. *Angew. Chem.-Int. Edit.* **54**, 1855-1858, doi:10.1002/anie.201410339 (2015).

11 Ong, W. Q., Citron, Y. R., Sekine, S. & Huang, B. Live Cell Imaging of Endogenous mRNA Using RNA-Based Fluorescence "Turn-On" Probe. *ACS Chem Biol* **12**, 200-205, doi:10.1021/acschembio.6b00586 (2017).

12 Bhadra, S. & Ellington, A. D. A Spinach molecular beacon triggered by strand displacement. *RNA* **20**, 1183-1194, doi:10.1261/rna.045047.114 (2014).

13 Furuhata, Y. *et al.* Programmable RNA detection with a fluorescent RNA aptamer using optimized three-way junction formation. *RNA* **25**, 590-599, doi:10.1261/rna.069062.118 (2019).

14 You, M. & Jaffrey, S. R. Structure and Mechanism of RNA Mimics of Green Fluorescent Protein. *Annu Rev Biophys* **44**, 187-206, doi:10.1146/annurev-biophys-060414-033954 (2015).

15 Zadeh, J. N. *et al.* NUPACK: Analysis and design of nucleic acid systems. *J Comput Chem* **32**, 170-173, doi:10.1002/jcc.21596 (2011).

16 WHO. World Malaria Report 2019. (2020).

17 Wampfler, R. *et al.* Strategies for detection of Plasmodium species gametocytes. *PLoS One* **8**, e76316-e76316, doi:10.1371/journal.pone.0076316 (2013).

18 Wheeler, S. S. *et al.* Surveillance for Western Equine Encephalitis, St. Louis Encephalitis, and West Nile Viruses Using Reverse Transcription Loop-Mediated Isothermal Amplification. *PLoS One* **11**, e0147962-e0147962, doi:10.1371/journal.pone.0147962 (2016).

19 Pardee, K. *et al.* Rapid, Low-Cost Detection of Zika Virus Using Programmable Biomolecular Components. *Cell* **165**, 1255-1266, doi:https://doi.org/10.1016/j.cell.2016.04.059 (2016).

20 Lanciotti, R. S. & Kerst, A. J. Nucleic acid sequence-based amplification assays for rapid detection of West Nile and St. Louis encephalitis viruses. *J. Clin. Microbiol.* **39**, 4506-4513, doi:10.1128/JCM.39.12.4506-4513.2001 (2001).

21 Delaunay, C. *et al.* Comparative selection of the K65R and M184V/I mutations in human immunodeficiency virus type 1-infected patients enrolled in a trial of first-line triple-nucleoside analog therapy (Tonus IMEA 021). *J Virol* **79**, 9572-9578, doi:10.1128/JVI.79.15.9572-9578.2005 (2005).

22 Ma, D., Shen, L., Wu, K., Diehnelt, C. W. & Green, A. A. Low-cost detection of norovirus using paper-based cell-free systems and synbody-based viral enrichment. *Synth Biol (Oxf)* **3**, ysy018, doi:10.1093/synbio/ysy018 (2018).

CHAPTER 3

A LOW-COST BROCCOLI APTASENSOR-BASED PLATFORM FOR DETECTING PATHOGEN NUCLEIC ACIDS

3.1 Introduction

As of 18 October, over 40 million confirmed cases of COVID-19 worldwide, with more than 1.1 million deaths have been reported by WHO. Similar to COVID-19, some of the life-threatening endemic diseases such as dengue fever and malaria, often have influenza-like symptoms[56,62,63]. Early diagnosis is essential for treatment and management of these diseases, as well as effectively containing outbreak spread. Conventional diagnosis including nucleic acid-based test via polymerase chain reaction (PCR); culture-based tests[64]; and rapid antigen-detection (RDT) tests[65]. Culture-based testing is time intensive and requires well-trained health workers. RDT tests are easy-to-use and provides rapid results, but are often ineffective for immunocompromised patients[66] and lack sensitivity and specificity. Although nucleic acid-based tests provide more accurate and more sensitive detections[67], they require expensive thermal cycling equipment for precise temperature control.

To overcome these limitations, our lab as a part of a multi-institution team developed a paper-based diagnostic platform for nucleic-acid detection that is rapid and low-cost[41,61]. It uses a riboregulator named a toehold switch[68] for the target RNA detection. NASBA[39], an isothermal RNA amplification technique, was added to reduce the limit of detection to three femtomolar. This diagnostic platform employs a cell-free transcription-translation system (freeze-dried onto paper disk[69]) for the expression of the reporter enzyme ß-galactosidase.

Here we describe an alternative RNA-based fluorescence output strategy that simplifies and substantially decreases the cost and time for pathogen nucleic acid detection. In the previous chapter, we developed Broccoli-based RNA aptasensors for detecting target RNA with no sequence constraints, with the best aptasensors providing ON/OFF ratios over 200-fold. In this chapter, we demonstrate the integration of three isothermal amplification techniques with Broccoli aptasensors for detecting pathogen DNA or RNA. Of these, a two-step NASBA-Broccoli

aptasensor assay was validated against dengue patient serum. Moreover, we established one-pot, single-step assays for pathogen RNA detection, which can potentially reduce contamination, shorten diagnostic test time and lower costs by avoiding the use of cell-free systems.

3.2 Materials and Methods

3.2.1 Screening of Broccoli-based RNA aptasensors

Six to eight promising designs identified during *in silico* aptasensor selection were tested for each pathogen target. Synthetic DNA (Integrated DNA Technologies) encoding the pathogen-specific Broccoli aptasensors was amplified by PCR (Phusion High-Fidelity PCR Master Mix with HF Buffer, NEB, M0531L). Aptasensor PCR products were purified by using MinElute PCR Purification Kit (Qiagen, 28006). Aptasensor RNA was transcribed using AmpliScribe™ T7-Flash™ Transcription Kit (Lucigen, ASF3507) from 0.1 μM of the DNA template at 37 °C for 2 hours. Target RNA was directly synthesized from PCR-amplified product and purified using RNA Clean & Concentrator™-25 columns (Zymo Research, R1017). A BioTek Synergy H1 Multi-Mode Reader was used for all plate reader measurements, approximately 0.5 μM or 2 μL of aptasensor RNA, 2.5 μM of purified target RNA were added to the 96 well plate along with 4 μM of DFHBI-1T (Lucerna, 410). DFHBI-1T buffer is consisted of 40 mM HEPES pH 7.4, 100 mM KCl, and 1 mM MgCl2. Before each measurement, samples were shaken linearly for 30 seconds to ensure proper mixing. The plate reader was preheated, and the measurements were taken at 37°C unless indicated otherwise.

3.2.2 Detection of target DNA amplified via LAMP

For target DNA amplification with LAMP, 1x Isothermal Amplification Buffer (NEB, B0537S), 1.4 mM dNTPs, 8 mM MgSO4, 1.6 μM FIP/BIP, 0.2 μM F3/B3, 0.4 μM LoopF/B primers, 0.32 U/μL (NEB, M0537L), 2 μL target DNA were mixed at 4°C and incubated at 65°C for 50 min. The final volume of the amplification reaction was 10 μL. After adding 0.5 μM of the primer tagged with a T7 promoter to the reaction, it was incubated for an additional 10 min at

65°C. 1 μL amplified product and 0.1 μM DNA template for the aptasensor were added to T7 transcription components along with 10 μM of DFHBI-1T. The mixture was then measured using a plate reader at 37°C for 2 hours.

3.2.3 Detection of target DNA amplified via RPA

For target DNA amplification with RPA, 1 μL target DNA, 0.48 μM forward and reverse primers, 5.9 μL rehydrated enzyme mix (TwistAmp® Basic), 0.2 μL T7 RNA polymerase (Lucigen), 2 mM rNTPs, 100U Protector RNase Inhibitor (Roche, 3335402001) and 2.5μM DFHBI-1T were mixed on ice. 0.5 μL of 280 mM MgAc was added to initiate the 10-μL amplification reaction. Samples were incubated at 37°C for 2 hours. The 5 μL of amplified target RNAs were mixed with 1 μL separately transcribed aptasensor RNA and 44 μL water for the plate reader measurement at 37°C for 6 hours.

For target RNA amplification with RPA, 1 μL target RNA, 0.48 μM forward and reverse primers, 29.5 μL rehydrated enzyme mix (TwistAmp® Basic RT), 0.2 μM DNA template, 1 μL T7 RNA polymerase, 2mM rNTPs, 100U Protector RNase Inhibitor and 10 μM DFHBI-1T were mixed on ice. 2.5 μL of 280 mM MgAc was added to initiate this 50 μL amplification reaction. Samples were incubated at 37°C for 2 hours before the plate reader measurement.

3.2.4 Isothermal amplification of target RNA with NASBA

For target RNA amplification with NASBA, reaction Buffer (Life Sciences, NEC-1-24; 33.5%), Nucleotide Mix (Life Sciences, NEC-1-24; 16.5%), Protector RNase Inhibitor (Roche; 0.5%), 12.5 mM of each NASBA primer (2%), nuclease free water (2.5%), and target RNA (20%) were mixed at 4°C and heated to 65°C for 2 min, followed by a 10 min incubation at 41°C. Enzyme Mix (Life Sciences, NEC-1-24; 25%) was then added to the reaction for a final volume of 6 μL. After mixing the reaction was incubated at 41°C for 2 hours. For one-pot reactions, 0.1 μM DNA sensor and 4 μM DFHBI-1T were added into the NASBA reaction. For a 35 μL two-pot reaction, 5 μL of

the NASBA amplified RNA product was combined with 0.7 μL of RNA aptasensor and 4 μM DFHBI-1T buffer. Sample incubated and measured at 37 °C for additional 2 hr.

3.2.5 Virus RNA Extraction for Clinical Dengue virus sample

The viral RNA was extracted by using QIAamp Viral RNA Mini Kit (Qiagen, 52904) according to the manufacturer's instructions. RNA was eluted with 60 μl Buffer AVE (Qiagen, 1020953) and stored at −80°C before use.

3.3 Results and Discussion

3.3.1 Detection of target DNA amplified via LAMP

We coupled Broccoli-based RNA sensor with isothermal amplification reactions to enable detection of target nucleic acids at lower concentrations. The first amplification technique we implemented was loop-mediated isothermal amplification (LAMP)[42]. LAMP is a DNA amplification method with an operating temperature of 60-65 °C, employs 2 to 3 pairs of primers and a strand-displacing DNA polymerase for primer extensions. The amplified DNA first forms a dumbbell-shaped DNA intermediate, and the final amplified product containing alternately inverted repeats of the target sequence. The complexity of the amplified target DNA structure can be a challenge for the aptasensor detection, so we designed our aptasensor targeting regions close to the loop of amplicon. We proposed a workflow for integrating LAMP amplicon (Fig. 3.1a), in which a target DNA is amplified using standard LAMP primers for 50 min at 65°C before the addition of a primer tagged with a T7 promoter sequence. This primer binds to the forward loop region (F2) and attaches the promoter site to the amplified DNA product so the amplicon can be transcribed for optimal aptasensor detection. After 10-min incubation at 65°C, the resulting DNA is then added to an *in vitro* T7 transcription reaction (Tx) containing aptasensor RNA and DFHBI-1T, and is measured using a plate reader for 2 hr at 37 °C.

To validate the successful integration of LAMP with Broccoli-based aptasensors, we designed and screened aptasensors for detecting Saint Louis encephalitis virus (SLEV), and the

best performing aptasensor (Fig. 3.1b) provided an ON/OFF of 25-fold after 2-hr detection. This aptasensor was chosen for the demonstration with target DNA concentration from 2,500,000 to 2.5 copies per LAMP reaction, and we found the limit of detection for our SLEV aptasensor-LAMP assay was at 25 copies per reaction (Fig. 3.1c). SLEV target region and LAMP primers were from previously reported diagnostic assays[58].

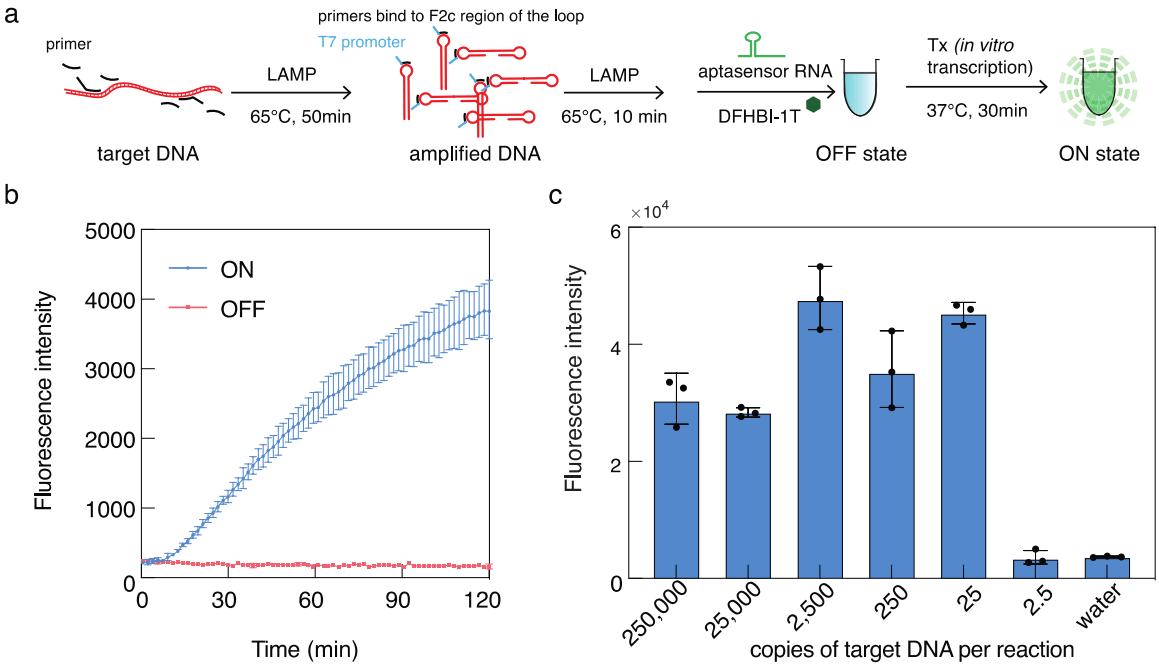

Figure 3.1 Detection of target DNA amplified via LAMP

(a) General workflow for detecting pathogen DNA amplified via LAMP using Broccoli-based aptasensors.

(b) Best aptasensor for detecting SLEV target RNA. The relative errors for the ON- and OFF-states are from the s.d. of n = 3 technical replicates.

(c) Detection limit measurements for synthetic SLEV target DNA subject to LAMP amplification plus *in vitro* transcription and detection using Broccoli-based aptasensor. The relative errors for the fluorescence intensities are from the s.d. of n = 3 technical replicates.

3.3.2 Detection of target DNA amplified via RPA

Next we demonstrated the incorporation of the recombinase polymerase amplification[46] (RPA) in a similar fashion. RPA amplifies DNA at a constant temperature of 37 °C and utilizes one pair of primers and three enzymes: a recombinase, a single-stranded DNA-binding protein (SSB) and strand-displacing DNA polymerase. We set up a workflow for detecting RNA amplicons from

RPA of DNA targets, where we coupled RPA with T7 transcription (Fig. 3.2a). To validate and this workflow, we designed aptasensor for valley fever detection. Valley fever, also known as coccidioidomycosis, is an infection caused by the fungi *Coccidioides posadasii* and *C immitis*. 40% of infections are symptomatic with influenza-like illness, and a small portion of patients developed life-threatening conditions. The time to diagnosis ranges from one day to more than four years[70]. There is a need for a low-cost, easy-to-use and sensitive diagnostic for Valley fever. We downloaded and aligned the genome sequences for *Coccidioides posadasii* from NCBI database, and selected several conserved regions as targets and designed hundreds of aptasensor. The best performing aptasensor exhibited ON/OFF over 200-fold (Fig. 3.2b). We were able to obtain a detection limit of 1 fM (Fig. 3.2c) with our proposed workflow. For these two detection assays described above, the amplification reaction and the detection reaction were carried out separately, so we referred to them as a two-step (two-pot) assay.

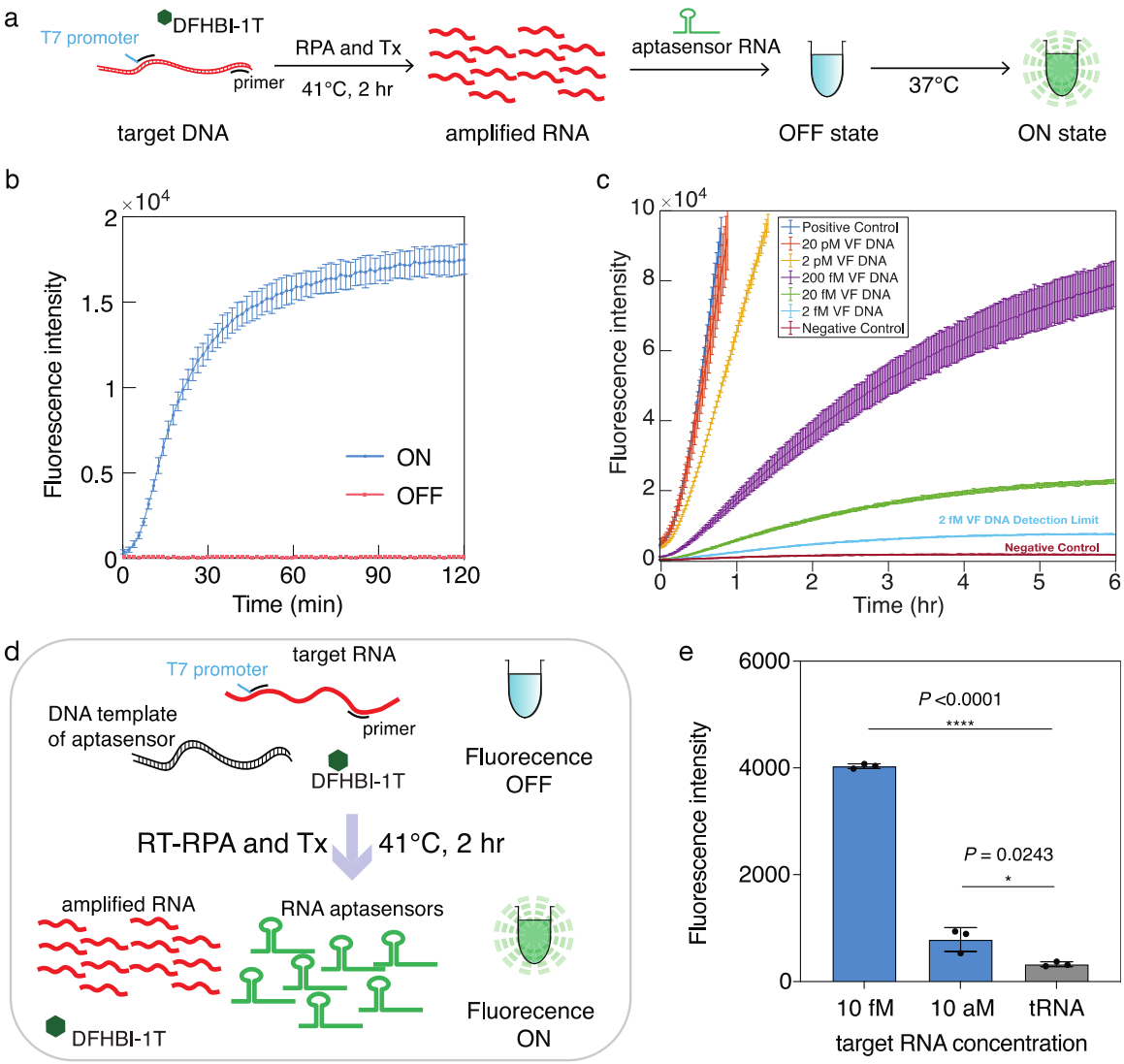

Figure 3.2 Detection of target DNA amplified via RPA

(a) Workflow for detecting pathogen DNA using Broccoli aptasensors via RPA. Target DNA is amplified via RPA and transcribed via T7 transcription in presence of DFHBI-1T. The resulting target RNA is combined with aptasensor for plate reader detection assay.

(b) Best aptasensor for detecting valley fever target RNA. The relative errors for the ON- and OFF-states are from the s.d. of n = 3 technical replicates.

(d) Detection limit measurements for synthetic Valley Fever target DNA subject to RPA amplification coupling *in vitro* T7 transcription and detection using Broccoli-based aptasensor.

(e) Workflow for detecting pathogen RNA using Broccoli aptasensors via one-pot RPA.

(f) Detection limit for synthetic *Pfs*25 target RNA subject to one-pot RPA/aptasensor assay.

The relative errors for the fluorescence intensities are from the s.d. of n = 3 biological replicates (two-tailed *t*-test; **P* < 0.05; *****P* < 0.0001).

RPA coupling reverse transcription (RT) and T7 transcription was previously reported[71] for detecting target nucleic acids with CRISPR nucleases, so we sought to develop a one-pot single

step assay, where all reaction steps including aptasensor transcription, target RNA amplification and the fluorescence detection occur simultaneously in a single reaction buffer at a single temperature. Previously screened and validated *Pfs*25_fwd aptasensor was used to verify this one-pot assay. Briefly, aptasensor DNA, target RNA, DFHBI-1T, primers, rNTPs, T7 polymerase were added to RT-RPA reaction components. Mixture was incubated at 42°C for 2 hr before measured using plate reader (Fig 3.2d). The sensitivity of the one-pot RPA reaction for detecting synthetic *Pfs*25 RNA was as low as 10 aM (Fig. 3.2e).

3.3.3 Detection of target RNA amplified via NASBA

Subsequently, we coupled Broccoli-based RNA sensors with an RNA isothermal amplification technique known as the nucleic acid sequence-based amplification (NASBA) which utilizes three enzymes: reverse transcriptase, RNase H and T7 RNA polymerase. We proposed a one-pot reaction which enables the amplification of target RNA and the transcription of aptasensor RNA simultaneously in a single reaction tube as illustrated in Figure 3.3a, as T7 polymerase was one of the NASBA reaction enzymes. We previously screened out aptasensors for *Pfs*25 gene detection, the best performing ones for sense target RNA (Fig 3.3b) and for antisense target RNA (Fig 3.3c) provided ON/OFF ratios exceeding 100-fold. To increase the yield of the RNA amplification reaction, inosine 5'-triphosphate is widely used for replacing approximately 25% of the canonical rGTP[72]. We tested the NASBA kit for *in vitro* transcription of the *Pfs*25 aptasensors and their cognate target RNA, and confirmed that they could provide the similar fluorescence as those obtained from RNAs with only canonical bases (Fig. 3.3d). We mixed 0.1 μM of the aptasensor DNA templates with NASBA reaction components (specified in Materials and Methods) with synthetic target RNA concentrations of 20 fM, 2 fM, and 0.2 fM, and used the water as the negative control. 4 μM of DFHBI-1T buffer and enzyme cocktail were added before a 2 hr incubation at 41°C. Figure 3f shows a photograph of the resulting samples excited under a blue light transilluminator using a blue-light filter to remove excess excitation light. The one-pot NASBA/

aptasensor assay enabled facile detection of Pfs25 RNA by eye down to 0.2 fM, which was 482 copies per reaction.

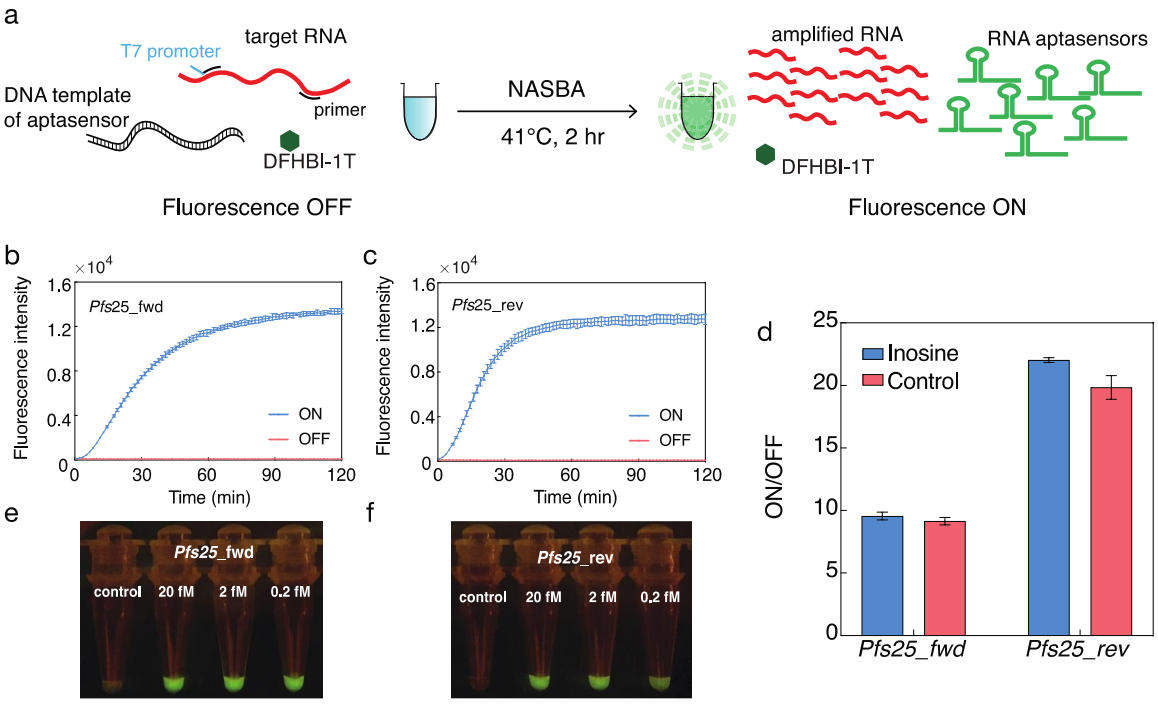

Figure 3.3 Detection of target RNA amplified via NASBA

(a) General workflow for detecting pathogen RNA amplified via NASBA using Broccoli-based aptasensors. **(b-c)** Best aptasensors for detecting *Pfs*25 target RNA in sensor (*Pfs*25_fwd) or antisense direction (*Pfs*25_rev). The relative errors for the ON- and OFF- states are from the s.d. of n = 3 biological replicates. **(d)** Inosine tolerance test. Broccoli-based aptasensor RNAs and their cognate target RNAs were transcribed using the NASBA kit and using the T7 transcription kit as control. **(e-f)** Detection for synthetic *Pfs*25 target RNA subject to NASBA amplification and detection using Broccoli-based aptasensor. Photograph were taken two hours using an iPhone. The resulting samples were excited under a blue light transilluminator, and excess excitation light were removed using a blue-light filter.

3.3.4 Detection of dengue viral RNA from clinical sample

We designed aptasensors for detecting RNA of dengue virus to demonstrate that our platform could be used to detect viral RNAs from clinical samples. Dengue is a mosquito-borne viral infection that is prevalent in tropical and sub-tropical area worldwide. With an estimate of 10,000 deaths and 100 million symptomatic infections per year, half of the world's population is at

risk of dengue[73]. We screened 48 aptasensors, the best performing aptasensor provided a strong ON/OFF ratio over 100 within 30 min (Fig. 3.4a). We chose this aptasensor for target RNA titration experiments and found the sensor displayed a linear response to target RNA concentration (Fig. 3.4b), and the sensor was activated with 30 nM target RNA. However, the reported viral RNA concentration of 10^6 copies/ml (1.7fM) in patient serum[74] was lower than the detection limit of the aptasensor. To determine the limit of detection for our assay incorporating an RNA isothermal amplification, we carried out a series of NASBA/aptasensor two-pot reactions (Fig. 3.4c) with synthetic dengue target RNA concentrations ranging from 200 fM down to 0.2 aM. Briefly, we amplified target RNA in a 20 μL NASBA reaction while transcribing aptasensor RNA separately. For the readout measurement using a plate reader, we mixed the 5-μL NASBA product, 1 μM aptasensor RNA, 4 μM DFHBI-1T buffer for a final volume of 35 μL. The fluorescence intensities of the aptasensors upon binding of the NASBA products for 30 min revealed that two-pot our dengue assay had a detection limit of 0.2 aM corresponding to 120 copies/mL (Fig. 3.4d).

We then applied the two-pot Broccoli-based aptasensor/NASBA assay to patient serum samples. Samples were collected from patients who took the serology test against the dengue virus. Virus RNA was extracted from sera with a viral RNA extraction kit, amplified via NASBA, combined with RNA aptasensor and DFHBI-1T and measured with a plate reader for 2 hours. All three positive patients tested positive for dengue virus-specific IgG, IgM antibodies and NS1 (non-structural protein) for dengue virus, and all negative patients tested all negative, and our results (Fig. 3.4e) agreed with the serological tests.

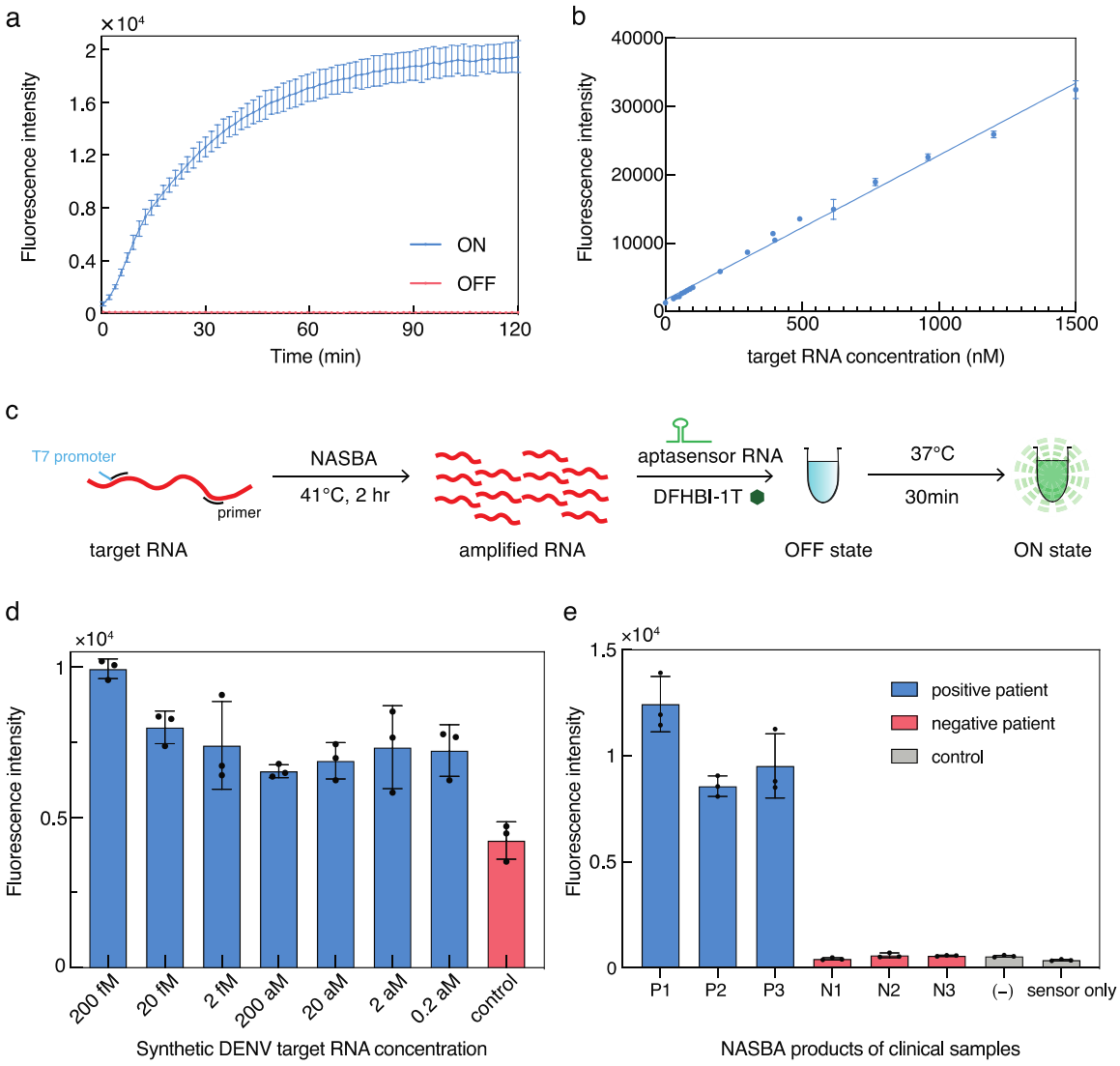

Figure 3.4 Broccoli aptasensor platform for dengue virus detection.

(a) Best aptasensor for detecting dengue. The relative errors for the ON- and OFF- states are from the s.d. of n = 3 biological replicates.

(b) Calibration curve for the dengue target RNA. The relative errors for the fluorescence intensities are from the s.d. of n = 3 technical replicates.

(c) Workflow for detecting pathogen RNA using our Broccoli-aptasensor diagnostic assay via NASBA amplification.

(d) Detection limit measurements for synthetic DENV target RNA subject to NASBA amplification and detection using Broccoli-based aptasensor. The relative errors for the fluorescence intensities are from the s.d. of n = 3 biological replicates.

(e) DENV target RNA detection for RNA extracted from patient serum. Measurements were taken after 2 hours of NABSA product detection. The relative errors for the fluorescence intensities are from the s.d. of n = 3 biological replicates.

3.4 Conclusion

We verified that our Broccoli-aptasensors were able to detect products from isothermal amplification LAMP, RPA, and NASBA, and developed Broccoli aptasensor-based detection assays for pathogen DNA or RNA targets. Th Broccoli-based diagnostic assay is low-cost, rapid, sensitive, high-throughput and easy-to-use. One-pot assays with RT-RPA-Tx or NASBA were able to detection of synthetic target RNA for *Pfs*25 within two hours with a limit of detection of 10 aM and 200 aM, repectively. Two-step assays with LAMP allowed the detection of synthetic target DNA for SLEV in less than three hours with a limit of detection of 2.5 copies/ reaction. Two-step assays with RPA detected 1 fM of synthetic DNA target for Valley fever in less than four hours. Two-step NASBA assay for dengue with a detection limit of 0.2 aM (120 copies/mL) synthetic target RNA was validated using clinical samples acquired from patients with dengue.

3.5 Reference

1 Cologna, R., Armstrong, P. M. & Rico-Hesse, R. Selection for virulent dengue viruses occurs in humans and mosquitoes. *J Virol* **79**, 853-859, doi:10.1128/JVI.79.2.853-859.2005 (2005).

2 WHO. World Malaria Report 2019. (2020).

3 Cunha, B. A. & Raza, M. During influenza season: all influenza-like illnesses are not due to influenza: dengue mimicking influenza. *J Emerg Med* **48**, e117-120, doi:10.1016/j.jemermed.2014.12.051 (2015).

4 Rajapaksha, P. *et al.* A review of methods for the detection of pathogenic microorganisms. *Analyst* **144**, 396-411, doi:10.1039/c8an01488d (2019).

5 Polley, S. *et al.* Clinical Evaluation of a LAMP test kit for Diagnosis of Imported Malaria. *The Journal of infectious diseases* **208**, doi:10.1093/infdis/jit183 (2013).

6 Abbasi, J. The Promise and Peril of Antibody Testing for COVID-19. *JAMA* **323**, 1881-1883, doi:10.1001/jama.2020.6170 (2020).

7 Pavšič, J. *et al.* Standardization of Nucleic Acid Tests for Clinical Measurements of Bacteria and Viruses. *J. Clin. Microbiol.* **53**, 2008-2014, doi:10.1128/JCM.02136-14 (2015).

8 Pardee, K. *et al.* Rapid, Low-Cost Detection of Zika Virus Using Programmable Biomolecular Components. *Cell* **165**, 1255-1266, doi:https://doi.org/10.1016/j.cell.2016.04.059 (2016).

9 Ma, D., Shen, L., Wu, K., Diehnelt, C. W. & Green, A. A. Low-cost detection of norovirus using paper-based cell-free systems and synbody-based viral enrichment. *Synth Biol (Oxf)* **3**, ysy018, doi:10.1093/synbio/ysy018 (2018).

10 Green, A. A., Silver, P. A., Collins, J. J. & Yin, P. Toehold switches: de-novo-designed regulators of gene expression. *Cell* **159**, 925-939, doi:10.1016/j.cell.2014.10.002 (2014).

11 Guatelli, J. C. *et al.* Isothermal, in vitro amplification of nucleic acids by a multienzyme reaction modeled after retroviral replication. *Proc Natl Acad Sci U S A* **87**, 1874-1878, doi:10.1073/pnas.87.5.1874 (1990).

12 Pardee, K. *et al.* Paper-based synthetic gene networks. *Cell* **159**, 940-954, doi:10.1016/j.cell.2014.10.004 (2014).

13 Notomi, T. *et al.* Loop-mediated isothermal amplification of DNA. *Nucleic Acids Res.* **28**, 7, doi:10.1093/nar/28.12.e63 (2000).

14 Wheeler, S. S. *et al.* Surveillance for Western Equine Encephalitis, St. Louis Encephalitis, and West Nile Viruses Using Reverse Transcription Loop-Mediated Isothermal Amplification. *PLoS One* **11**, e0147962-e0147962, doi:10.1371/journal.pone.0147962 (2016).

15 Piepenburg, O., Williams, C. H., Stemple, D. L. & Armes, N. A. DNA Detection Using Recombination Proteins. *PLOS Biology* **4**, e204, doi:10.1371/journal.pbio.0040204 (2006).

16 Benedict, K. *et al.* Enhanced Surveillance for Coccidioidomycosis, 14 US States, 2016. *Emerging Infectious Disease journal* **24**, 1444, doi:10.3201/eid2408.171595 (2018).

17 Kellner, M. J., Koob, J. G., Gootenberg, J. S., Abudayyeh, O. O. & Zhang, F. SHERLOCK: nucleic acid detection with CRISPR nucleases. *Nature Protocols* **14**, 2986-3012, doi:10.1038/s41596-019-0210-2 (2019).

18 Nakahara, K., Hataya, T. & Uyeda, I. Inosine 5'-triphosphate can dramatically increase the yield of NASBA products targeting GC-rich and intramolecular base-paired viroid RNA. *Nucleic Acids Res.* **26**, 1854-1856, doi:10.1093/nar/26.7.1854 (1998).

19 Messina, J. P. *et al.* The current and future global distribution and population at risk of dengue. *Nat. Microbiol* **4**, 1508-1515, doi:10.1038/s41564-019-0476-8 (2019).

20 Laue, T., Emmerich, P. & Schmitz, H. Detection of dengue virus RNA in patients after primary or secondary dengue infection by using the TaqMan automated amplification system. *J. Clin. Microbiol.* **37**, 2543-2547, doi:10.1128/JCM.37.8.2543-2547.1999 (1999).

CHAPTER 4

PROGRAMMING SYNTHESIS OF NONRIBOSOMAL PEPTIDES USING RNA

4.1 Introduction

Nonribosomal peptides (NRP) are structurally diverse and pharmaceutically important natural products that include the antibiotic daptomycin[75], the anticancer agent bleomycin[76], and the immunosuppressant cyclosporine[77]. NRPs are assembled by modular enzyme complexes called nonribosomal peptide synthetases (NRPS). Each module of the synthetase is responsible for adding a specific amino acid onto the peptide, and there are catalytic domains within each module for the activation, formation, elongation, and, in some cases, termination of the peptide[78]. A typical module contains an adenylation (A) domain for the recognizing and activating the amino acid substrate; a thiolation (T) or peptidyl carrier protein (PCP) domain for transferring intermediate between the catalytic domains; and a condensation (C) domain for catalyzing the amide bond formation. This assembly-line organization offers potential for rational design and modification of peptide via substitution of substrate-specific modules (or domains). Moreover, the ability to incorporate non-proteinogenic amino acids makes NRPS desirable targets for bioengineering. However, engineering nonribosomal peptide synthetase is challenging. Current attempts are mostly focused on protein engineering via rational protein design and directed evolution[79-81].

In this chapter, using the well-studied biosynthetic pathway of enterobactin[82] as the model**,** we developed RNA scaffolds to control the assembly of NRPS enzymes. While the wild-type *E. coli* operon comprises the enzymes EntE, EntB, and EntF, we generated a functional chimeric assembly by replacing the EntB protein with the DhbB protein from *B. subtilis* during reconstitution of the enterobactin pathway. Assembly is driven an RNA scaffold generated by pRNA-x motifs derived from the 3-way junction of a bacteriophage packaging RNA (pRNA)[83]. The helix arms were modified with kissing loop (KL) sequences to hybridize with other pRNA-x motifs having complementary KL sequences, and with peptide binding-RNA aptamer on the other axial arm for protein fusion attachment. An RNA-binding peptide was fused onto the N-terminus of the NRPS for

pairing with RNA scaffolds. In the presence of the RNA scaffold pair, the DhbB protein along with EntE and EntF was able to produce a yield 56.4% of the full wild-type EntEBF pathway.

4.2 Material and Methods

4.2.1 Materials, General Methods, and Instrumentation

E. coli strains were propagated in LB liquid medium or on LB agar plates with the appropriate antibiotic selection. The following *E. coli* strains were used in this chapter: BL21 Star DE3 (F− ompT hsdSB (rB−mB−) gal dcm rne131 (DE3), MG1655Pro (F− λ− ilvG- rfb-50 rph-1 SpR lacR tetR), and DH5α (endA1 recA1 gyrA96 thi-1 glnV44 relA1 hsdR17(rK−mK+) λ−; Invitrogen). *E. coli* strain BAP1 (BL21(DE3) ΔprpRBCD::T7prom-sfp,T7prom-prpE) and Plasmid pTEV5, gifted to us by Prof. Michael Thomas (University of Wisconsin), were used for all protein expression and construction. Oligonucleotide primers were synthesized by Integrated DNA Technologies. Phusion High-Fidelity PCR Master Mix with HF Buffer, restriction enzymes and T4 DNA ligase were purchased from New England Biolabs. All other chemicals were purchased from Sigma-Aldrich. BioTek Synergy H1 Multi-Mode Reader was used for all plate reader measurements. Liquid chromatography (LC)-MS analysis was carried out on Agilent 6530 Quadrupole Time-of-Flight LC/MS System using a using a C18 column. The identities of all DNA fragments amplified by PCR were confirmed by DNA sequencing (DNASU Sequencing Core Facility at ASU and GENEWIZ).

4.2.2 Plasmid construction

Plasmids were constructed by PCR and Gibson assembly techniques. EntE, EntB and EntF genes were amplified from chromosomal DNA of *E coli*. MG1655Pro strain and cloned into the cloning site of pTEV5. Dhb, DhbB and DhbF genes gifted to us were on vectors without His-tag, and we subcloned their genes or gene fragments into pTEV5 vector. To construct peptide-fused proteins, single-stranded DNA templates for RNA binding peptides were purchased and amplified using PCR. The amplified double-stranded DNAs were then inserted in between of the His-tag and the N-terminus of the Ent/Dhb proteins by a 30-bp homology domains using Gibson

assembly[84]. All Gibson assembly products were transformed in the *E. coli* DH5α strain and then sent out for sequence validation via Sanger sequencing.

4.2.3 Protein Expression and Purification

To overproduce E and B proteins, 500 mL LB (supplemented carbenicillin) cultures of *E.coli* BL21 Star (DE3) strain and *E.coli* BAP1 BL21 (DE3) strain, respectively. For over production F proteins, *E. coli* BAP1 BL21(DE3) strain was transformed with pACYC-Duet-BSU31959 and pTEV5-EntF or pTEV5-DhbF. Transformants were selected on LB medium containing carbenicillin and chloramphenicol. Culture was at 30 °C until an OD600 of ~ 0.6 was reached. The temperature was reduced to 16 °C and cells were shaken for 1 hr before adding isopropyl β-D-1-thiogalactopyranoside (IPTG; 60 μM) and further grown for 16-20 hr at 16 °C. Cells were harvested by centrifugation (20 min at 4800 rpm) and stored in -80 °C for at least 2 hr. They were then resuspended in buffer A (Tris-HCl pH8.0 [50 mM], NaCl [300 mM], TCEP [1 mM], imidazole [10 mM]) containing cOmplete™ Protease Inhibitor Cocktail (Roche). The cells were broken by ultrasonication (pulses of 1-sec on, 2-sec off for a total of 10 mins at 10% amplitude) on ice. Cell debris was removed by centrifugation (30 min at 30,000 rcf). Clarified supernatant was purified using His-tag affinity chromatography (HisTrap™ High Performance, Sigma). Purified protein was dialyzed in dialysis buffer (40 mM Tris–HCl [pH 8.0, adjusted at room temperature (RT)], 200 mM NaCl, and 1 mM dithiothreitol [DTT]) and stored in 50 % glycerol at -20 °C or -80 °C for long term storage.

4.2.4 RNA Synthesis

All the DNA oligonucleotides were designed using NUPACK and purchased from IDT. PCR was used for amplification of the DNA strands. For *in vitro* transcriptions, AmpliScribe™ T7-Flash™ Transcription Kit (Epicenter) was used according to the manufacturer's instruction. The concentration of DNA template added into each individual transcription reaction was approximately 0.1 μM. DNase I was used to remove excess DNA template for the termination of the transcription**,**

then RNA Clean & Concentrator™ (Zymo Research) was used for further purification. The concentration of each of the RNA scaffolds after purification was approximately 50 µM.

4.2.5 RNA Gel shift assays

All the RNA strands were annealed individually by heating at 95 ^{o}C for 3 mins and slowly cooled down to 37 °C. Different pairs (cognate and non-cognate) were then combined at 1:1 concentration at 0.5 uM and incubated at 37 ^{o}C for 30 mins in reaction buffer I (50 mM Tris, 50 mM KCl at pH 8.0). The interactions between kissing loop RNA strands were characterized by shift in the bands compared to the individual strands when run on 5% native PAGE gels with 50 mM KCl and 1 mM $MgCl_2$. All the gels were run for approx. 1 hr at 37 ^{o}C. To test the interaction between NRPS fused with RNA binding peptides and its cognate aptamer fused into pRNA-x structure, the RNA strands were annealed and incubated as described earlier. To these 2 uM of NRPS protein in reaction buffer II (50 mM Tris, 50 mM KCl, 5 mM $MgCl_2$ at pH 8.0) was added and incubated for 1 hr at 37 ^{o}C. It was further characterized on 5% native PAGE gels run for 2 hr at 37 ^{o}C.

4.2.6 *In vitro* enterobactin reconstitution assay

Each 40-µL reaction mixture contained 75 mM Tris pH 7.5, 10 mM MgCl2, 0.5 mM DTT, 10 mM DHB, 500 nM L-serine, 10 mM ATP, 1.5 micromolar BSU31959 1 nM EntE, 1 microM EntB or DhbB and 1 microM EntF. The reaction is carried out at 37 ^{o}C for 17 hours before analysis.

For reconstitution assay with RNA scaffolds, the NRPS-peptide fusion and and its cognate RNA were incubated at 1:1 molar ratio in 75 mM Tris pH 7.5, 10 mM MgCl2, 50 mM KCl, 1U/µL Protector RNase inhibitor (Roche), and 0.5 mM DTT for 1 hour at 37 ^{o}C before mix with the rest of the components mentioned above.

For chrome azurol S (CAS) liquid assay, a 30 µL sample was mixed with 120 µL CAS reagent, incubated at room temperature for 5 min before measured using plate reader at 630 nm. Triplicate experiments were performed. For LC-MS analysis, sample is quenched with an equal volume 1 mM HCl. 750 µL ethyl acetate was added to the quench reaction, and 500 µL was

removed and concentrated. The residue was resuspended in 50 µL with 30% acetonitrile and 0.1% formic acid in H2O, and 10 µL of each sample was analyzed by LCMS.

4.3 Results and Discussion

4.3.1 Biosynthesis of enterobactin.

Enterobactin is a siderophore, a small iron-chelator secreted by *E. coli* and other gram negative bacteria under iron-starvation[85]. The enterobactin biosynthesis scheme[82] for *E coli.* is shown in Fig 4.1.1a. The synthetase consists of three proteins: EntE, EntB and EntF. EntE is a stand-alone A domain that activates 2,3-dihydroxybenzoate (DHB). The two-domain protein EntB contains an N-terminal isochorismate lyase (ICL) domain, and a C-terminal aryl carrier protein (ArCP) onto which DHB is loaded. The ICL domain is involved in production of DHB, but it is not essential for *in vitro* production of enterobactin[82], and ArCP domain interacts with EntE and C domain in EntF. EntF is a four-domain protein that includes, from N- to C-terminus: a C domain that catalyses the formation of the amide bond between DHB and the loaded serine; an A domain that activates serine and loads it onto the ArCP domain; and a thioesterase (TE) domain that produces the macrolactone trimer of 2,3-dihydroxybenzoyl-serine.

The non-cognate ArCP domain we chose is from the siderophore assembly line of bacillibactin from *B. subtilis*[86]. Similar to the enterobactin synthetases there are also three proteins in this system for making a macrolactone trimer of 2,3-dihydroxybenzoyl-glycine-threonine (Fig. 4.1b). DhbE and DhbB are very similar functionally and structurally to EntE and EntB, respectively. DhbF is a two-module protein with two sets of C, A, and PCP domains and a terminal TE domain. The posttranslational modification of the carrier protein domains by a phosphopantetheinyl transferase (PPTase) is also required for both synthetases. EntD protein is the PPTase specifically for *E coli, whereas* Sfp protein from *B. subtilis* is a broad-substrate PPTase[87]. Therefore, we used *E.coli* BAP1 strain containing a chromosomal insertion of Sfp for the overproduction of PCP/ArCP proteins.

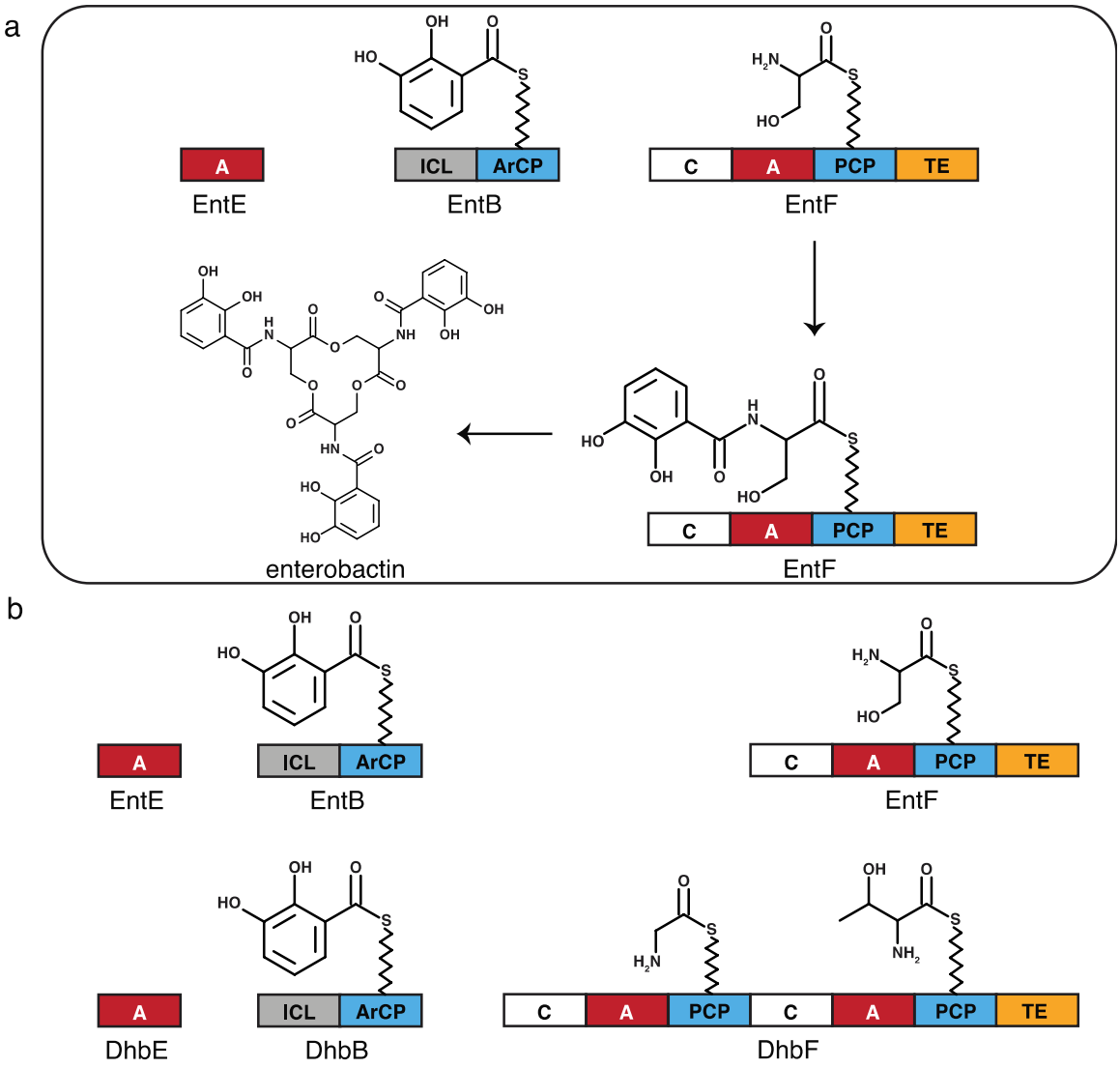

Figure 4.1 Siderophore biosynthesis modules from *E. coli* (Ent) and *B. subtilis* (Dhb)
(a) Enterobactin biosynthesis scheme.
(b) Comparison of domain organization of synthetases for enterobactin and bacillibactin.

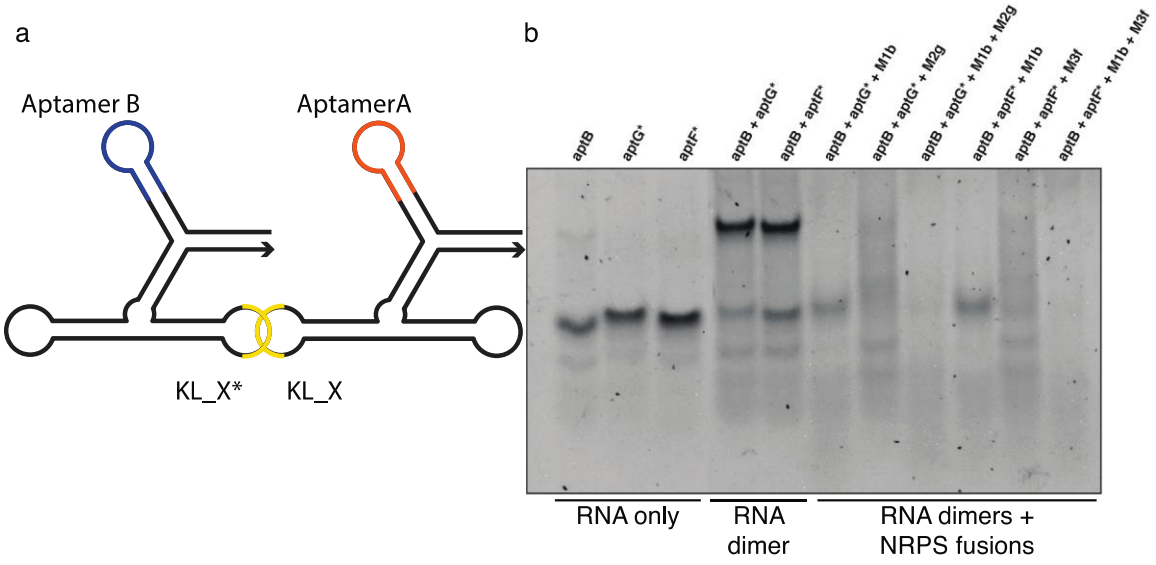

Figure 4.2. Design and Characterization of the RNA scaffolds.
(a) Secondary structure of the RNA scaffold pairs. The RNA scaffolds are hybridized via kissing loop (KL) interactions. The complementary sequences of the kissing loops are indicated in yellow. **(B)** PAGE gel image for RNA gel-shift assay. Abbreviations: apt, aptamer; B and b, Biv-tat RNA and peptide; G and g, P22N RNA aptamer and peptide; F and f, lambdaN(G1N2R4); M, module; M1 licB1; M2 and M3, licA1. (licA1 and licB1 are NRPS modules from *B. licheniformis.)*

4.3.2 Design and characterization of the RNA scaffolds

To employ RNA for the arrangement and enhancement of the interactions between the non-cognate DhbB and EntE and EntF, we designed an RNA scaffold with the secondary structure shown in Figure 4.2a. We used the pRNA x-motif[83] as the core of the RNA scaffold which serves as a sticky end to link other functional RNA with no effects on its folding. For each pair of RNA scaffolds, we modified helix arms with complementary HIV kissing loop sequences and different peptide-binding RNA aptamers. As result, each RNA scaffold can bind to its cognate peptide-NRPS fusion, and two RNA scaffolds can hybridize to one another in linear kissing loop junctions[88]. Since we located the kissing loop sequences on the coaxial arms of the pRNA structure, the RNA scaffolds should form co-linear assemblies after kissing loop interactions. The kissing loop sequence could be located not only on any of the two coaxial arms, but also on both arms for higher order assemblies of RNA scaffolds. For scaffold pairs, we put poly-A sequences on the vacant arm to prevent the nonspecific interactions.

We used RNA gel-shift assays to assess the dimerization of the RNA scaffolds as well as the binding between the RNA scaffold and peptide fused NRPS proteins. RNA scaffolds were separately annealed before combining at 1:1 concentrations. We found that RNA scaffolds formed dimers when scaffold pairs with complementary kissing loops were combined (Fig. 4.2b). Wide-type kissing loop sequences were used in these pairs. Moreover, we confirmed the interaction between the RNA dimer and their cognate protein fusions.

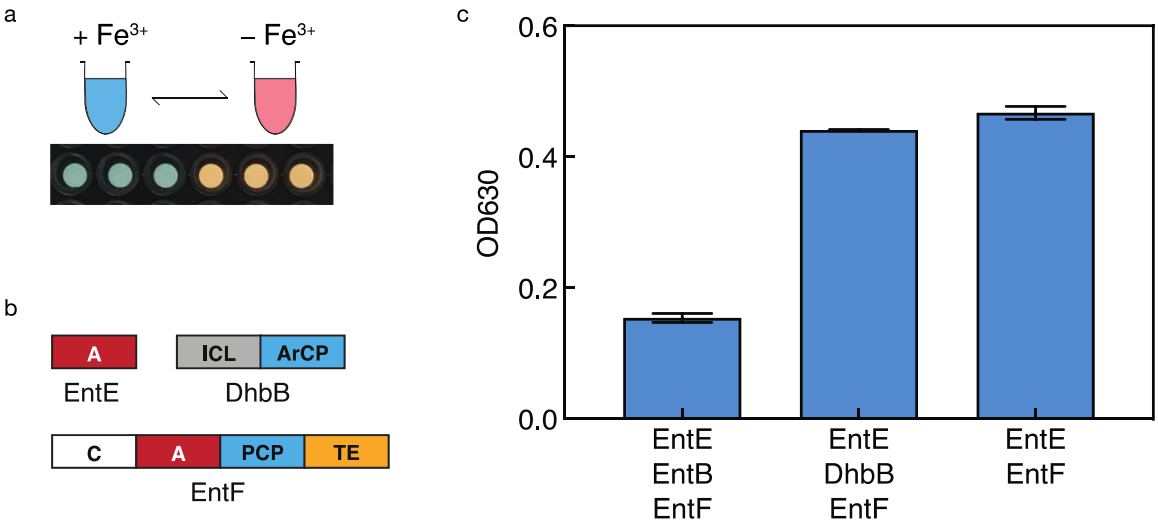

Figure 4.3 Characterization of the swapped domain.
(a) CAS assay for measuring siderophore production. A color change is observed when iron is chelated by the siderophore.
(b) Schematic showing the domain arrangement used for initial characterization.
(c) *In vitro* enterobactin production measured using CAS assay. EntEBF was the positive control, and EntEF was the negative control. The relative errors for the ON- and OFF- states are from the s.d. of n = 3 replicates.

4.3.3 Initial characterization of DhbB and protein production.

Chrome azurol S (CAS) assay[89] was used for the detection and quantification of the enterobactin production. The CAS reaction contains the CAS dye, iron, and a detergent (hexadecyl-trimethylammonium bromide). When enterobactin chelates and removes the iron from the iron-CAS-detergent complex, a color change from blue to orange is observed (Fig. 4.3a). For the reconstitution of the enterobactin we swapped DhbB with EntB (Fig. 4.3b), we found that there is a

91.6% decrease in the enterobactin production (Fig. 4.3c). This result indicates that there is little to no interaction between non-cognate DhbB and EntE and EntF. The enterobactin produced by our purified EntEBF proteins was verified using LC/MS.

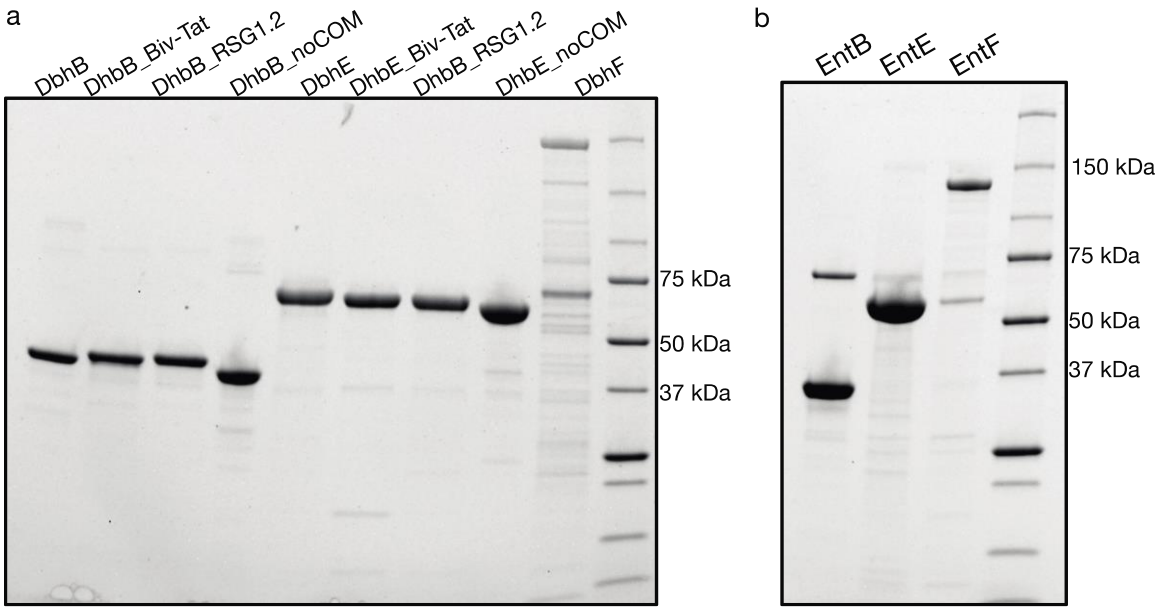

Figure 4.4 SDS-PAGE gel images for purified proteins.
(a) Purified DhbB proteins wild type, peptide fusions and communication domain removeds.
(b) Purified EntE, EntB and EnF proteins.

Next, we fused peptide for binding the RNA aptamers onto DhbB (Fig. 4.4a) and EntE and EntF. Communication-mediating (COM) domain is observed in some NRPS systems for establishing binding between proteins, and it is located at the termini[90]. We thus removed several N-terminal residues from DhbB upstream to the ICL domain to generate DhbB lacking a COM domain (DhbB_noCOM). NRPS protein construction, expression and purification was challenging because of their size. The molecular weight for EntF (a four-domain protein) is 143 kDa, and 264 kDa for the two-module DhbF protein. The SDS-PAGE gel for the purified EntEBF proteins is shown in Figure 4.4b.

4.3.4 Co-localization of proteins using RNA scaffolds.

We designed RNA scaffolds pairs with various peptide binding RNA aptamers and original HIV kissing loop sequences (KL1 and KL1*). For EntF-Biv_tat and noCOM_DhbB-BMV_gag fusions, we had RNA scaffolds, (KL1-BMV_Gag) and (KL1*-Biv_tat). To investigate the effectiveness our RNA scaffolds, we performed enterobactin reconstitution assays in vitro. CAS assays were then used for quantification of enterobactin production (Fig. 4.5a). Wild-type EntEBF was the positive control, and EntEF was the negative control which was used as reference for the quantitative estimation of siderophore production (Fig. 4.5b) [91]. We found that there was a 42.9% increase in enterobactin production compared with no RNA system (Fig. 4.5c), and a 48.0% increase compared with unmodified EntE, dhbB and EntF system.

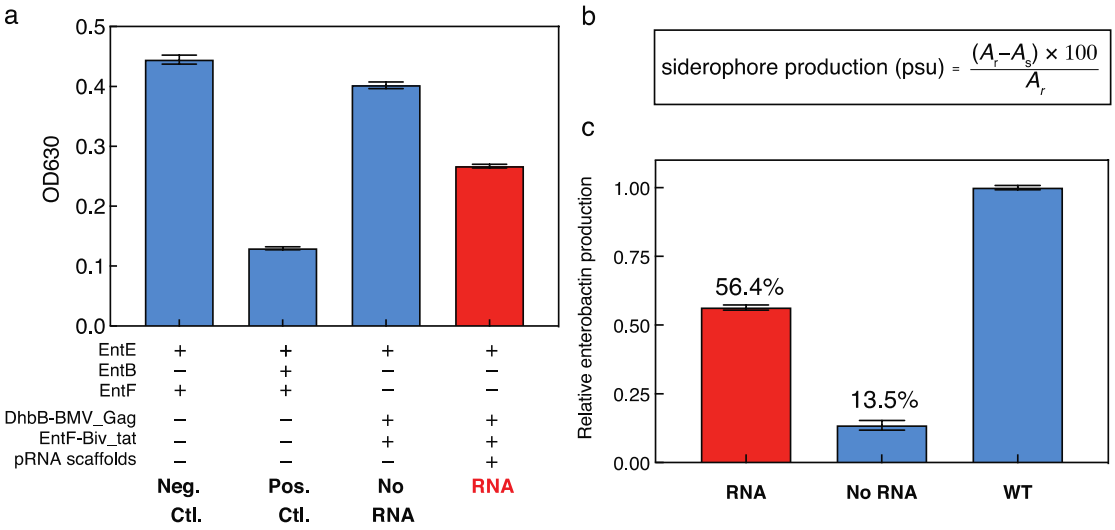

Figure 4.5 *In vitro* enterobactin reconstitution with RNA scaffold.
(a) Enterobactin production measured using CAS assay.
(b) Formular used for quantitative estimation of siderophore production with CAS assay, where A_r is the reference absorbance (CAS solution and negative control), and A_s is the sample absorbance (CAS solution and sample).
(c) Relative yields compared to wild-type EntEBF.
The relative errors for the ON- and OFF- states are from the s.d. of n = 3 replicates.

4.4 Conclusion

To assess the portability of the modules/domains/proteins between assembly lines, we replaced the dual domain protein EntB (ICL-ArCP) from the *E. coli* with dual domain protein DhbB

(ICL-ArCP) from the *B. subtilis*. We constructed a pairs of RNA scaffolds to enhance the protein-protein recognitions between the noncognate proteins DhbB and EnF, and facilitated the *in vitro* production of enterobactin. The best RNA scaffold pair provided a 418% increase in enterobactin production compared with the system in absence of the RNA scaffold, and reached approximately 56% of the activity of the wild-type enzyme assembly.

4.5 Reference

1 Miao, V. *et al.* Daptomycin biosynthesis in Streptomyces roseosporus: cloning and analysis of the gene cluster and revision of peptide stereochemistry. *Microbiology* **151**, 1507-1523, doi:https://doi.org/10.1099/mic.0.27757-0 (2005).

2 Du, L., Sánchez, C., Chen, M., Edwards, D. J. & Shen, B. The biosynthetic gene cluster for the antitumor drug bleomycin from Streptomyces verticillus ATCC15003 supporting functional interactions between nonribosomal peptide synthetases and a polyketide synthase. *Chem Biol* **7**, 623-642, doi:10.1016/s1074-5521(00)00011-9 (2000).

3 Lawen, A. Biosynthesis of cyclosporins and other natural peptidyl prolyl cis/trans isomerase inhibitors. *Biochimica et Biophysica Acta (BBA) - General Subjects* **1850**, 2111-2120, doi:https://doi.org/10.1016/j.bbagen.2014.12.009 (2015).

4 Fischbach, M. A. & Walsh, C. T. Assembly-Line Enzymology for Polyketide and Nonribosomal Peptide Antibiotics: Logic, Machinery, and Mechanisms. *Chemical Reviews* **106**, 3468-3496, doi:10.1021/cr0503097 (2006).

5 Bozhüyük, K. A. J. *et al.* De novo design and engineering of non-ribosomal peptide synthetases. *Nature Chemistry* **10**, 275-281, doi:10.1038/nchem.2890 (2018).

6 Zhou, Z., Lai, J. R. & Walsh, C. T. Directed evolution of aryl carrier proteins in the enterobactin synthetase. *Proceedings of the National Academy of Sciences* **104**, 11621-11626, doi:10.1073/pnas.0705122104 (2007).

7 Kries, H., Niquille, D. L. & Hilvert, D. A Subdomain Swap Strategy for Reengineering Nonribosomal Peptides. *Chemistry & Biology* **22**, 640-648, doi:https://doi.org/10.1016/j.chembiol.2015.04.015 (2015).

8 Gehring, A. M., Mori, I. & Walsh, C. T. Reconstitution and characterization of the Escherichia coli enterobactin synthetase from EntB, EntE, and EntF. *Biochemistry* **37**, 2648-2659, doi:10.1021/bi9726584 (1998).

9 Haque, F. *et al.* Ultrastable synergistic tetravalent RNA nanoparticles for targeting to cancers. *Nano Today* **7**, 245-257, doi:https://doi.org/10.1016/j.nantod.2012.06.010 (2012).

10 Gibson, D. G. *et al.* Enzymatic assembly of DNA molecules up to several hundred kilobases. *Nature Methods* **6**, 343-345, doi:10.1038/nmeth.1318 (2009).

11 Raymond, K. N., Dertz, E. A. & Kim, S. S. Enterobactin: An archetype for microbial iron transport. *Proceedings of the National Academy of Sciences* **100**, 3584-3588, doi:10.1073/pnas.0630018100 (2003).

12 May, J. J., Wendrich, T. M. & Marahiel, M. A. The dhb operon of Bacillus subtilis encodes the biosynthetic template for the catecholic siderophore 2,3-dihydroxybenzoate-glycine-threonine trimeric ester bacillibactin. *J Biol Chem* **276**, 7209-7217, doi:10.1074/jbc.M009140200 (2001).

13 Quadri, L. E. *et al.* Characterization of Sfp, a Bacillus subtilis phosphopantetheinyl transferase for peptidyl carrier protein domains in peptide synthetases. *Biochemistry* **37**, 1585-1595, doi:10.1021/bi9719861 (1998).

14 Ennifar, E., Walter, P., Ehresmann, B., Ehresmann, C. & Dumas, P. Crystal structures of coaxially stacked kissing complexes of the HIV-1 RNA dimerization initiation site. *Nature Structural Biology* **8**, 1064-1068, doi:10.1038/nsb727 (2001).

15 Schwyn, B. & Neilands, J. B. Universal chemical assay for the detection and determination of siderophores. *Anal Biochem* **160**, 47-56, doi:10.1016/0003-2697(87)90612-9 (1987).

16 Hahn, M. & Stachelhaus, T. Selective interaction between nonribosomal peptide synthetases is facilitated by short communication-mediating domains. *Proceedings of the National Academy of Sciences of the United States of America* **101**, 15585-15590, doi:10.1073/pnas.0404932101 (2004).

17 Payne, S. M. Iron acquisition in microbial pathogenesis. *Trends Microbiol* **1**, 66-69, doi:10.1016/0966-842x(93)90036-q (1993).

CHAPTER 5

CONCLUSION AND FUTURE DIRECTIONS

Since the development of RNA aptamers in 1990, researchers have made immense advances in the past three decades. An RNA aptamer (Pegaptanib [(Macugen; Pfizer/Eyetech)])[92] has been approved by the U.S. Food and Drug Administration for clinical use to treat age-related macular degeneration. With new approaches for generating aptamers, a great number of aptamer targeting ions, organic molecules, proteins, viruses, parasites, and animals have been selected. This dissertation focuses on studying the applications for the fluorogenic and peptide-binding RNA aptamers by constructing fluorogenic aptamer-based biosensors and colocalizing proteins using peptide-binding aptamer modified RNA scaffolds.

First, in three approaches fluorogenic RNA aptamer Broccoli were engineered into a biosensor as a readout for detecting target RNA. These aptamer-based biosensors, or aptasensors, have no sequence constraints for their target RNA. They are similar to a molecular beacon, as they are initially nonfluorescent in absence of their cognate RNA, and only become fluorescent when bound to their cognate target RNA. The best design strategy employs a toehold-initiated strand displacement, and was used for later studies. Most of these aptasensors can become fully active in 30~60 min upon target RNA hybridization. Several design improvements might improve the rate of activation, including extending the length of the toehold region, increasing the number of the bulges in the stem, enlarging the size of the bulges and/or the size of the loop, and shortening the length of the stem. We expect reductions in detection time can be obtained with further optimizations as these parameters could have negative impact on the signal leakage. RNA aptasensors were generated for targeting seven different pathogens, with two of them providing ON/OFF ratios over 100-fold in 30 min. The high dynamic range and low signal leakage of the aptasensors could expand its potential applications such as *in vivo* sensors for mRNA visualization. Moreover, Broccoli aptasensors could also be easily adapt for small molecule detection by coupling them with another RNA aptamer at the 5’ end near the toehold region. Future studies should be

centered on increasing the specificity and orthogonality of the aptasensor for possible usage in single-nucleotide polymorphisms detection.

Second, diagnostic assays were developed incorporating isothermal amplification with Broccoli aptasensors. Nucleic acid concentrations in clinical sample (femtomolar range) is lower than the Limit of Detection (LoD) for Broccoli (nanomolar range). To increase the sensitivity of the aptasensor, an amplification method is required. Isothermal amplification methods were investigated, because they require less sophisticated instrumentation and are more suitable for resource-limited areas. The four chosen pathogens were two viruses, one parasite and one fugus, and they were responsible for epidemic and endemic infections (dengue, Saint Louis encephalitis, malaria and valley fever). Amplicons from LAMP, RPA, RT-PRA, and NASBA reactions were all detectable by the Broccoli aptasensor. Coupling with LAMP, we were able to detect 25 copies of synthetic SLEV DNA per reaction in less than 90 min. There are two disadvantages of LAMP reactions: 1) sensitivity to contamination and 2) optimal working temperature ranging from 60 to 65°C. To prevent contamination, we used two different working areas for sample handling and heat inactivated the LAMP reaction before the detection step. If we lower the reaction temperature for LAMP to 56°C and use a T7 polymerase that is active from 37-56°C, then we can possibly establish a one-pot assay for detecting nucleic acids within in one hour. Many next-generation nucleic acid-based tests including SHERLOCK and paper-based tests[41,93] require a separate amplification step before the detection step. A one-step test in principle will save time and prevent foreseeable contaminations from sample transfer. We were able to establish one-pot assays incorporating NASBA and RT-RPA-TX for detecting target RNA in two hours with LoD at 10 aM and 200 aM, respectively. Two-step NASBA assay had a LoD of 0.2 aM for synthetic RNA target (dengue), and was validated by clinical sample from patients tested for dengue. Although the two-step NASBA assay was more sensitive, it took a longer time overall compare with one-pot NASBA assay. Unlike the other two methods mentioned earlier, the detection step for Broccoli aptasensor was not enzymatic which means there's no signal amplification at this step. The low sensitivity for one-pot

NASBA and RPA reactions could be due to low RNA aptasensor (low readout). One-pot buffer optimization would be helpful for aptamer-DFHBI-1T complex conformation and enzymatic activity.

Third, RNA scaffolds were constructed with peptide-binding RNA aptamers enabling the colocalization of chimeric proteins for in vitro reconstitution of enterobactin. We chose the enterobactin biosynthesis pathway as a model for better understanding of protein assembly on RNA scaffolds via peptide-binding aptamers. Two RNA motifs were used for constructing the scaffolds: pRNA-x motif and kissing loop hairpins. pRNA-x was the core, and kissing loop sequences were modified on the coaxial helixes which allowed the collinear assembly of the scaffolds. In vitro studies suggest that RNA scaffolds were able to enhance the protein-protein interaction between DhbB and EntF. The best RNA scaffolds provide a 418% increase in enterobactin production compared with the system in absence of the scaffolds. To better understand these results, future studies should explore higher order assembly of RNA scaffolds by controlling the EntE protein. Only few studies[94] have demonstrated using RNA scaffolds for controlling protein assembly *in vivo*. It is sensible to validate the RNA scaffolds in *E coli* as our next step.

5.1 Reference

1 Gragoudas, E. S., Adamis, A. P., Cunningham, E. T., Jr., Feinsod, M. & Guyer, D. R. Pegaptanib for neovascular age-related macular degeneration. *N Engl J Med* **351**, 2805-2816, doi:10.1056/NEJMoa042760 (2004).

2 Joung, J. *et al.* Point-of-care testing for COVID-19 using SHERLOCK diagnostics. *medRxiv*, 2020.2005.2004.20091231, doi:10.1101/2020.05.04.20091231 (2020).

3 Pardee, K. *et al.* Rapid, Low-Cost Detection of Zika Virus Using Programmable Biomolecular Components. *Cell* **165**, 1255-1266, (2016).

4 Sachdeva, G., Garg, A., Godding, D., Way, J. C. & Silver, P. A. In vivo co-localization of enzymes on RNA scaffolds increases metabolic production in a geometrically dependent manner. *Nucleic Acids Res.* **42**, 9493-9503, doi:10.1093/nar/gku617 (2014).

REFERENCES

CHAPTER 1

1 Ellington, A. D. & Szostak, J. W. In vitro selection of RNA molecules that bind specific ligands. *Nature* **346**, 818-822, doi:10.1038/346818a0 (1990).

2 Tuerk, C. & Gold, L. Systematic evolution of ligands by exponential enrichment: RNA ligands to bacteriophage T4 DNA polymerase. *Science* **249**, 505-510, doi:10.1126/science.2200121 (1990).

3 Nutiu, R. & Li, Y. In vitro selection of structure-switching signaling aptamers. *Angew Chem Int Ed Engl* **44**, 1061-1065, doi:10.1002/anie.200461848 (2005).

4 Chang, Y. C. *et al.* Identification and characterization of oligonucleotides that inhibit Toll-like receptor 2-associated immune responses. *Faseb j* **23**, 3078-3088, doi:10.1096/fj.09-129312 (2009).

5 Sefah, K., Shangguan, D., Xiong, X., O'Donoghue, M. B. & Tan, W. Development of DNA aptamers using Cell-SELEX. *Nat Protoc* **5**, 1169-1185, doi:10.1038/nprot.2010.66 (2010).

6 Cheng, C., Chen, Y. H., Lennox, K. A., Behlke, M. A. & Davidson, B. L. In vivo SELEX for Identification of Brain-penetrating Aptamers. *Mol Ther Nucleic Acids* **2**, e67, doi:10.1038/mtna.2012.59 (2013).

7 Fukuda, K. *et al.* Specific RNA aptamers to NS3 protease domain of hepatitis C virus. *Nucleic Acids Symp Ser*, 237-238 (1997).

8 Kumar, P. K. *et al.* Isolation of RNA aptamers specific to the NS3 protein of hepatitis C virus from a pool of completely random RNA. *Virology* **237**, 270-282, doi:10.1006/viro.1997.8773 (1997).

9 Gopinath, S. C., Kawasaki, K. & Kumar, P. K. Selection of RNA-aptamer against human influenza B virus. *Nucleic Acids Symp Ser (Oxf)*, 85-86, doi:10.1093/nass/49.1.85 (2005).

10 Jang, K. J., Lee, N. R., Yeo, W. S., Jeong, Y. J. & Kim, D. E. Isolation of inhibitory RNA aptamers against severe acute respiratory syndrome (SARS) coronavirus NTPase/Helicase. *Biochem Biophys Res Commun* **366**, 738-744, doi:10.1016/j.bbrc.2007.12.020 (2008).

11 Barfod, A., Persson, T. & Lindh, J. In vitro selection of RNA aptamers against a conserved region of the Plasmodium falciparum erythrocyte membrane protein 1. *Parasitol Res* **105**, 1557-1566, doi:10.1007/s00436-009-1583-x (2009).

12 Homann, M. & Göringer, H. U. Uptake and intracellular transport of RNA aptamers in African trypanosomes suggest therapeutic "piggy-back" approach. *Bioorg Med Chem* **9**, 2571-2580, doi:10.1016/s0968-0896(01)00032-3 (2001).

13 Nagarkatti, R., de Araujo, F. F., Gupta, C. & Debrabant, A. Aptamer based, non-PCR, non-serological detection of Chagas disease biomarkers in Trypanosoma cruzi infected mice. *PLoS Negl Trop Dis* **8**, e2650, doi:10.1371/journal.pntd.0002650 (2014).

14 Pan, Q. *et al.* Novel RNA aptamers targeting gastrointestinal cancer biomarkers CEA, CA50 and CA72-4 with superior affinity and specificity. *PLoS One* **13**, e0198980, doi:10.1371/journal.pone.0198980 (2018).

15 Rankin, C. J., Fuller, E. N., Hamor, K. H., Gabarra, S. A. & Shields, T. P. A Simple Fluorescent Biosensor for Theophylline Based on its RNA Aptamer. *Nucleosides, Nucleotides & Nucleic Acids* **25**, 1407-1424, doi:10.1080/15257770600919084 (2006).

16 Endoh, T. *et al.* Detection of Bioactive Small Molecules by Fluorescent Resonance Energy Transfer (FRET) in RNA−Protein Conjugates. *Bioconjugate Chemistry* **20**, 2242-2246, doi:10.1021/bc9002184 (2009).

17 Dwidar, M. & Yokobayashi, Y. Development of a histamine aptasensor for food safety monitoring. *Scientific Reports* **9**, 16659, doi:10.1038/s41598-019-52876-1 (2019).

18 Ling, K. *et al.* A self-assembling RNA aptamer-based nanoparticle sensor for fluorometric detection of Neomycin B in milk. *Anal Bioanal Chem* **408**, 3593-3600, doi:10.1007/s00216-016-9441-z (2016).

19 Jiang, H., Ling, K., Tao, X. & Zhang, Q. Theophylline detection in serum using a self-assembling RNA aptamer-based gold nanoparticle sensor. *Biosensors and Bioelectronics* **70**, 299-303, doi:https://doi.org/10.1016/j.bios.2015.03.054 (2015).

20 Paige, J. S., Wu, K. Y. & Jaffrey, S. R. RNA mimics of green fluorescent protein. *Science* **333**, 642-646, doi:10.1126/science.1207339 (2011).

21 Paige, J. S., Nguyen-Duc, T., Song, W. & Jaffrey, S. R. Fluorescence imaging of cellular metabolites with RNA. *Science* **335**, 1194, doi:10.1126/science.1218298 (2012).

22 Song, W., Strack, R. L. & Jaffrey, S. R. Imaging bacterial protein expression using genetically encoded RNA sensors. *Nat Methods* **10**, 873-875, doi:10.1038/nmeth.2568 (2013).

23 Strack, R. L., Song, W. & Jaffrey, S. R. Using Spinach-based sensors for fluorescence imaging of intracellular metabolites and proteins in living bacteria. *Nat Protoc* **9**, 146-155, doi:10.1038/nprot.2014.001 (2014).

24 You, M., Litke, J. L. & Jaffrey, S. R. Imaging metabolite dynamics in living cells using a Spinach-based riboswitch. *Proc Natl Acad Sci U S A* **112**, E2756-2765, doi:10.1073/pnas.1504354112 (2015).

25 Svensen, N. & Jaffrey, S. R. Fluorescent RNA Aptamers as a Tool to Study RNA-Modifying Enzymes. *Cell Chem Biol* **23**, 415-425, doi:10.1016/j.chembiol.2015.11.018 (2016).

26 Ong, W. Q., Citron, Y. R., Sekine, S. & Huang, B. Live Cell Imaging of Endogenous mRNA Using RNA-Based Fluorescence "Turn-On" Probe. *ACS Chem Biol* **12**, 200-205, doi:10.1021/acschembio.6b00586 (2017).

27 Aw, S. S., Tang, M. X., Teo, Y. N. & Cohen, S. M. A conformation-induced fluorescence method for microRNA detection. *Nucleic Acids Res* **44**, e92, doi:10.1093/nar/gkw108 (2016).

28 Bhadra, S. & Ellington, A. D. A Spinach molecular beacon triggered by strand displacement. *RNA* **20**, 1183-1194, doi:10.1261/rna.045047.114 (2014).

29 Akter, F. & Yokobayashi, Y. RNA signal amplifier circuit with integrated fluorescence output. *ACS Synth Biol* **4**, 655-658, doi:10.1021/sb500314r (2015).

30 Ying, Z. M., Wu, Z., Tu, B., Tan, W. & Jiang, J. H. Genetically Encoded Fluorescent RNA Sensor for Ratiometric Imaging of MicroRNA in Living Tumor Cells. *J Am Chem Soc* **139**, 9779-9782, doi:10.1021/jacs.7b04527 (2017).

31 Huang, K. *et al.* FASTmiR: an RNA-based sensor for in vitro quantification and live-cell localization of small RNAs. *Nucleic Acids Res.* **45**, doi:10.1093/nar/gkx504 (2017).

32 Kikuchi, N. & Kolpashchikov, D. M. Split Spinach Aptamer for Highly Selective Recognition of DNA and RNA at Ambient Temperatures. *Chembiochem* **17**, 1589-1592, doi:10.1002/cbic.201600323 (2016).

33 Song, W. *et al.* Imaging RNA polymerase III transcription using a photostable RNA-fluorophore complex. *Nat Chem Biol* **13**, 1187-1194, doi:10.1038/nchembio.2477 (2017).

34 Alam, K. K., Tawiah, K. D., Lichte, M. F., Porciani, D. & Burke, D. H. A Fluorescent Split Aptamer for Visualizing RNA-RNA Assembly In Vivo. *ACS Synth Biol* **6**, 1710-1721, doi:10.1021/acssynbio.7b00059 (2017).

35 Kolpashchikov, D. M. Binary Malachite Green Aptamer for Fluorescent Detection of Nucleic Acids. *Journal of the American Chemical Society* **127**, 12442-12443, doi:10.1021/ja0529788 (2005).

36 Dolgosheina, E. V. *et al.* RNA mango aptamer-fluorophore: a bright, high-affinity complex for RNA labeling and tracking. *ACS Chem Biol* **9**, 2412-2420, doi:10.1021/cb500499x (2014).

37 Sato, S. *et al.* Live-Cell Imaging of Endogenous mRNAs with a Small Molecule. *Angew. Chem.-Int. Edit.* **54**, 1855-1858, doi:10.1002/anie.201410339 (2015).

38 Huang, H. *et al.* A G-quadruplex-containing RNA activates fluorescence in a GFP-like fluorophore. *Nat. Chem. Biol.* **10**, 686-U128, doi:10.1038/nchembio.1561 (2014).

39 Guatelli, J. C. *et al.* Isothermal, in vitro amplification of nucleic acids by a multienzyme reaction modeled after retroviral replication. *Proc Natl Acad Sci U S A* **87**, 1874-1878, doi:10.1073/pnas.87.5.1874 (1990).

40 Burchill, S. A., Perebolte, L., Johnston, C., Top, B. & Selby, P. Comparison of the RNA-amplification based methods RT-PCR and NASBA for the detection of circulating tumour cells. *Br J Cancer* **86**, 102-109, doi:10.1038/sj.bjc.6600014 (2002).

41 Pardee, K. *et al.* Rapid, Low-Cost Detection of Zika Virus Using Programmable Biomolecular Components. *Cell* **165**, 1255-1266, (2016).

42 Notomi, T. *et al.* Loop-mediated isothermal amplification of DNA. *Nucleic Acids Res.* **28**, 7, doi:10.1093/nar/28.12.e63 (2000).

43 Zhao, Y., Chen, F., Li, Q., Wang, L. & Fan, C. Isothermal Amplification of Nucleic Acids. *Chem Rev* **115**, 12491-12545, doi:10.1021/acs.chemrev.5b00428 (2015).

44 Goto, M., Honda, E., Ogura, A., Nomoto, A. & Hanaki, K. Colorimetric detection of loop-mediated isothermal amplification reaction by using hydroxy naphthol blue. *Biotechniques* **46**, 167-172, doi:10.2144/000113072 (2009).

45 Xing, W. *et al.* Field evaluation of a recombinase polymerase amplification assay for the diagnosis of Schistosoma japonicum infection in Hunan province of China. *BMC Infect Dis* **17**, 164, doi:10.1186/s12879-017-2182-6 (2017).

46 Piepenburg, O., Williams, C. H., Stemple, D. L. & Armes, N. A. DNA Detection Using Recombination Proteins. *PLOS Biology* **4**, e204, doi:10.1371/journal.pbio.0040204 (2006).

47 Li, Y., Fan, P., Zhou, S. & Zhang, L. Loop-mediated isothermal amplification (LAMP): A novel rapid detection platform for pathogens. *Microb Pathog* **107**, 54-61, doi:10.1016/j.micpath.2017.03.016 (2017).

48 Cao, Y. *et al.* Development of a real-time fluorescence loop-mediated isothermal amplification assay for rapid and quantitative detection of Ustilago maydis. *Sci Rep* **7**, 13394, doi:10.1038/s41598-017-13881-4 (2017).

49 Oriero, E. C., Jacobs, J., Van Geertruyden, J. P., Nwakanma, D. & D'Alessandro, U. Molecular-based isothermal tests for field diagnosis of malaria and their potential contribution to malaria elimination. *J Antimicrob Chemother* **70**, 2-13, doi:10.1093/jac/dku343 (2015).

50 Lobato, I. M. & O'Sullivan, C. K. Recombinase polymerase amplification: Basics, applications and recent advances. *Trends Analyt Chem* **98**, 19-35, doi:10.1016/j.trac.2017.10.015 (2018).

51 Moore, M. D. & Jaykus, L. A. Development of a Recombinase Polymerase Amplification Assay for Detection of Epidemic Human Noroviruses. *Sci Rep* **7**, 40244, doi:10.1038/srep40244 (2017).

CHAPTER 2

1 Ellington, A. D. & Szostak, J. W. In vitro selection of RNA molecules that bind specific ligands. *Nature* **346**, 818-822, doi:10.1038/346818a0 (1990).

2 Tuerk, C. & Gold, L. Systematic evolution of ligands by exponential enrichment: RNA ligands to bacteriophage T4 DNA polymerase. *Science* **249**, 505-510, doi:10.1126/science.2200121 (1990).

3 Paige, J. S., Wu, K. Y. & Jaffrey, S. R. RNA mimics of green fluorescent protein. *Science* **333**, 642-646, doi:10.1126/science.1207339 (2011).

4 Filonov, G. S., Moon, J. D., Svensen, N. & Jaffrey, S. R. Broccoli: Rapid Selection of an RNA Mimic of Green Fluorescent Protein by Fluorescence-Based Selection and Directed Evolution. *Journal of the American Chemical Society* **136**, 16299-16308, doi:10.1021/ja508478x (2014).

5 Paige, J. S., Nguyen-Duc, T., Song, W. & Jaffrey, S. R. Fluorescence imaging of cellular metabolites with RNA. *Science* **335**, 1194, doi:10.1126/science.1218298 (2012).

6 Song, W., Strack, R. L. & Jaffrey, S. R. Imaging bacterial protein expression using genetically encoded RNA sensors. *Nat Methods* **10**, 873-875, doi:10.1038/nmeth.2568 (2013).

7 Strack, R. L., Song, W. & Jaffrey, S. R. Using Spinach-based sensors for fluorescence imaging of intracellular metabolites and proteins in living bacteria. *Nat Protoc* **9**, 146-155, doi:10.1038/nprot.2014.001 (2014).

8 You, M., Litke, J. L. & Jaffrey, S. R. Imaging metabolite dynamics in living cells using a Spinach-based riboswitch. *Proc Natl Acad Sci U S A* **112**, E2756-2765, doi:10.1073/pnas.1504354112 (2015).

9 Svensen, N. & Jaffrey, S. R. Fluorescent RNA Aptamers as a Tool to Study RNA-Modifying Enzymes. *Cell Chem Biol* **23**, 415-425, doi:10.1016/j.chembiol.2015.11.018 (2016).

10 Sato, S. *et al.* Live-Cell Imaging of Endogenous mRNAs with a Small Molecule. *Angew. Chem.-Int. Edit.* **54**, 1855-1858, doi:10.1002/anie.201410339 (2015).

11 Ong, W. Q., Citron, Y. R., Sekine, S. & Huang, B. Live Cell Imaging of Endogenous mRNA Using RNA-Based Fluorescence "Turn-On" Probe. *ACS Chem Biol* **12**, 200-205, doi:10.1021/acschembio.6b00586 (2017).

12 Bhadra, S. & Ellington, A. D. A Spinach molecular beacon triggered by strand displacement. *RNA* **20**, 1183-1194, doi:10.1261/rna.045047.114 (2014).

13 Furuhata, Y. *et al.* Programmable RNA detection with a fluorescent RNA aptamer using optimized three-way junction formation. *RNA* **25**, 590-599, doi:10.1261/rna.069062.118 (2019).

14 You, M. & Jaffrey, S. R. Structure and Mechanism of RNA Mimics of Green Fluorescent Protein. *Annu Rev Biophys* **44**, 187-206, doi:10.1146/annurev-biophys-060414-033954 (2015).

15 Zadeh, J. N. *et al.* NUPACK: Analysis and design of nucleic acid systems. *J Comput Chem* **32**, 170-173, doi:10.1002/jcc.21596 (2011).

16 WHO. World Malaria Report 2019. (2020).

17 Wampfler, R. *et al.* Strategies for detection of Plasmodium species gametocytes. *PLoS One* **8**, e76316-e76316, doi:10.1371/journal.pone.0076316 (2013).

18 Wheeler, S. S. *et al.* Surveillance for Western Equine Encephalitis, St. Louis Encephalitis, and West Nile Viruses Using Reverse Transcription Loop-Mediated Isothermal Amplification. *PLoS One* **11**, e0147962-e0147962, doi:10.1371/journal.pone.0147962 (2016).

19 Pardee, K. *et al.* Rapid, Low-Cost Detection of Zika Virus Using Programmable Biomolecular Components. *Cell* **165**, 1255-1266, doi:https://doi.org/10.1016/j.cell.2016.04.059 (2016).

20 Lanciotti, R. S. & Kerst, A. J. Nucleic acid sequence-based amplification assays for rapid detection of West Nile and St. Louis encephalitis viruses. *J. Clin. Microbiol.* **39**, 4506-4513, doi:10.1128/JCM.39.12.4506-4513.2001 (2001).

21 Delaunay, C. *et al.* Comparative selection of the K65R and M184V/I mutations in human immunodeficiency virus type 1-infected patients enrolled in a trial of first-line triple-

nucleoside analog therapy (Tonus IMEA 021). *J Virol* **79**, 9572-9578, doi:10.1128/JVI.79.15.9572-9578.2005 (2005).

22 Ma, D., Shen, L., Wu, K., Diehnelt, C. W. & Green, A. A. Low-cost detection of norovirus using paper-based cell-free systems and synbody-based viral enrichment. *Synth Biol (Oxf)* **3**, ysy018, doi:10.1093/synbio/ysy018 (2018).

CHAPTER 3

1 Cologna, R., Armstrong, P. M. & Rico-Hesse, R. Selection for virulent dengue viruses occurs in humans and mosquitoes. *J Virol* **79**, 853-859, doi:10.1128/JVI.79.2.853-859.2005 (2005).

2 WHO. World Malaria Report 2019. (2020).

3 Cunha, B. A. & Raza, M. During influenza season: all influenza-like illnesses are not due to influenza: dengue mimicking influenza. *J Emerg Med* **48**, e117-120, doi:10.1016/j.jemermed.2014.12.051 (2015).

4 Rajapaksha, P. *et al.* A review of methods for the detection of pathogenic microorganisms. *Analyst* **144**, 396-411, doi:10.1039/c8an01488d (2019).

5 Polley, S. *et al.* Clinical Evaluation of a LAMP test kit for Diagnosis of Imported Malaria. *The Journal of infectious diseases* **208**, doi:10.1093/infdis/jit183 (2013).

6 Abbasi, J. The Promise and Peril of Antibody Testing for COVID-19. *JAMA* **323**, 1881-1883, doi:10.1001/jama.2020.6170 (2020).

7 Pavšič, J. *et al.* Standardization of Nucleic Acid Tests for Clinical Measurements of Bacteria and Viruses. *J. Clin. Microbiol.* **53**, 2008-2014, doi:10.1128/JCM.02136-14 (2015).

8 Pardee, K. *et al.* Rapid, Low-Cost Detection of Zika Virus Using Programmable Biomolecular Components. *Cell* **165**, 1255-1266, doi:https://doi.org/10.1016/j.cell.2016.04.059 (2016).

9 Ma, D., Shen, L., Wu, K., Diehnelt, C. W. & Green, A. A. Low-cost detection of norovirus using paper-based cell-free systems and synbody-based viral enrichment. *Synth Biol (Oxf)* **3**, ysy018, doi:10.1093/synbio/ysy018 (2018).

10 Green, A. A., Silver, P. A., Collins, J. J. & Yin, P. Toehold switches: de-novo-designed regulators of gene expression. *Cell* **159**, 925-939, doi:10.1016/j.cell.2014.10.002 (2014).

11 Guatelli, J. C. *et al.* Isothermal, in vitro amplification of nucleic acids by a multienzyme reaction modeled after retroviral replication. *Proc Natl Acad Sci U S A* **87**, 1874-1878, doi:10.1073/pnas.87.5.1874 (1990).

12 Pardee, K. *et al.* Paper-based synthetic gene networks. *Cell* **159**, 940-954, doi:10.1016/j.cell.2014.10.004 (2014).

13 Notomi, T. *et al.* Loop-mediated isothermal amplification of DNA. *Nucleic Acids Res.* **28**, 7, doi:10.1093/nar/28.12.e63 (2000).

14 Wheeler, S. S. *et al.* Surveillance for Western Equine Encephalitis, St. Louis Encephalitis, and West Nile Viruses Using Reverse Transcription Loop-Mediated Isothermal Amplification. *PLoS One* **11**, e0147962-e0147962, doi:10.1371/journal.pone.0147962 (2016).

15 Piepenburg, O., Williams, C. H., Stemple, D. L. & Armes, N. A. DNA Detection Using Recombination Proteins. *PLOS Biology* **4**, e204, doi:10.1371/journal.pbio.0040204 (2006).

16 Benedict, K. *et al.* Enhanced Surveillance for Coccidioidomycosis, 14 US States, 2016. *Emerging Infectious Disease journal* **24**, 1444, doi:10.3201/eid2408.171595 (2018).

17 Kellner, M. J., Koob, J. G., Gootenberg, J. S., Abudayyeh, O. O. & Zhang, F. SHERLOCK: nucleic acid detection with CRISPR nucleases. *Nature Protocols* **14**, 2986-3012, doi:10.1038/s41596-019-0210-2 (2019).

18 Nakahara, K., Hataya, T. & Uyeda, I. Inosine 5'-triphosphate can dramatically increase the yield of NASBA products targeting GC-rich and intramolecular base-paired viroid RNA. *Nucleic Acids Res.* **26**, 1854-1856, doi:10.1093/nar/26.7.1854 (1998).

19 Messina, J. P. *et al.* The current and future global distribution and population at risk of dengue. *Nat. Microbiol* **4**, 1508-1515, doi:10.1038/s41564-019-0476-8 (2019).

20 Laue, T., Emmerich, P. & Schmitz, H. Detection of dengue virus RNA in patients after primary or secondary dengue infection by using the TaqMan automated amplification system. *J. Clin. Microbiol.* **37**, 2543-2547, doi:10.1128/JCM.37.8.2543-2547.1999 (1999).

CHAPTER 4

Miao, V. *et al.* Daptomycin biosynthesis in Streptomyces roseosporus: cloning and analysis of the gene cluster and revision of peptide stereochemistry. *Microbiology* **151**, 1507-1523, doi:https://doi.org/10.1099/mic.0.27757-0 (2005).

2 Du, L., Sánchez, C., Chen, M., Edwards, D. J. & Shen, B. The biosynthetic gene cluster for the antitumor drug bleomycin from Streptomyces verticillus ATCC15003 supporting functional interactions between nonribosomal peptide synthetases and a polyketide synthase. *Chem Biol* **7**, 623-642, doi:10.1016/s1074-5521(00)00011-9 (2000).

3 Lawen, A. Biosynthesis of cyclosporins and other natural peptidyl prolyl cis/trans isomerase inhibitors. *Biochimica et Biophysica Acta (BBA) - General Subjects* **1850**, 2111-2120, doi:https://doi.org/10.1016/j.bbagen.2014.12.009 (2015).

4 Fischbach, M. A. & Walsh, C. T. Assembly-Line Enzymology for Polyketide and Nonribosomal Peptide Antibiotics: Logic, Machinery, and Mechanisms. *Chemical Reviews* **106**, 3468-3496, doi:10.1021/cr0503097 (2006).

5 Bozhüyük, K. A. J. *et al.* De novo design and engineering of non-ribosomal peptide synthetases. *Nature Chemistry* **10**, 275-281, doi:10.1038/nchem.2890 (2018).

6 Zhou, Z., Lai, J. R. & Walsh, C. T. Directed evolution of aryl carrier proteins in the enterobactin synthetase. *Proceedings of the National Academy of Sciences* **104**, 11621-11626, doi:10.1073/pnas.0705122104 (2007).

7 Kries, H., Niquille, D. L. & Hilvert, D. A Subdomain Swap Strategy for Reengineering Nonribosomal Peptides. *Chemistry & Biology* **22**, 640-648, doi:https://doi.org/10.1016/j.chembiol.2015.04.015 (2015).

8 Gehring, A. M., Mori, I. & Walsh, C. T. Reconstitution and characterization of the Escherichia coli enterobactin synthetase from EntB, EntE, and EntF. *Biochemistry* **37**, 2648-2659, doi:10.1021/bi9726584 (1998).

9 Haque, F. *et al.* Ultrastable synergistic tetravalent RNA nanoparticles for targeting to cancers. *Nano Today* **7**, 245-257, doi:https://doi.org/10.1016/j.nantod.2012.06.010 (2012).

10 Gibson, D. G. *et al.* Enzymatic assembly of DNA molecules up to several hundred kilobases. *Nature Methods* **6**, 343-345, doi:10.1038/nmeth.1318 (2009).

11 Raymond, K. N., Dertz, E. A. & Kim, S. S. Enterobactin: An archetype for microbial iron transport. *Proceedings of the National Academy of Sciences* **100**, 3584-3588, doi:10.1073/pnas.0630018100 (2003).

12 May, J. J., Wendrich, T. M. & Marahiel, M. A. The dhb operon of Bacillus subtilis encodes the biosynthetic template for the catecholic siderophore 2,3-dihydroxybenzoate-glycine-threonine trimeric ester bacillibactin. *J Biol Chem* **276**, 7209-7217, doi:10.1074/jbc.M009140200 (2001).

13 Quadri, L. E. *et al.* Characterization of Sfp, a Bacillus subtilis phosphopantetheinyl transferase for peptidyl carrier protein domains in peptide synthetases. *Biochemistry* **37**, 1585-1595, doi:10.1021/bi9719861 (1998).

14 Ennifar, E., Walter, P., Ehresmann, B., Ehresmann, C. & Dumas, P. Crystal structures of coaxially stacked kissing complexes of the HIV-1 RNA dimerization initiation site. *Nature Structural Biology* **8**, 1064-1068, doi:10.1038/nsb727 (2001).

15 Schwyn, B. & Neilands, J. B. Universal chemical assay for the detection and determination of siderophores. *Anal Biochem* **160**, 47-56, doi:10.1016/0003-2697(87)90612-9 (1987).

16 Hahn, M. & Stachelhaus, T. Selective interaction between nonribosomal peptide synthetases is facilitated by short communication-mediating domains. *Proceedings of the National Academy of Sciences of the United States of America* **101**, 15585-15590, doi:10.1073/pnas.0404932101 (2004).

17 Payne, S. M. Iron acquisition in microbial pathogenesis. *Trends Microbiol* **1**, 66-69, doi:10.1016/0966-842x(93)90036-q (1993).

CHAPTER 5

1 Gragoudas, E. S., Adamis, A. P., Cunningham, E. T., Jr., Feinsod, M. & Guyer, D. R. Pegaptanib for neovascular age-related macular degeneration. *N Engl J Med* **351**, 2805-2816, doi:10.1056/NEJMoa042760 (2004).

2 Joung, J. *et al.* Point-of-care testing for COVID-19 using SHERLOCK diagnostics. *medRxiv*, 2020.2005.2004.20091231, doi:10.1101/2020.05.04.20091231 (2020).

3 Pardee, K. *et al.* Rapid, Low-Cost Detection of Zika Virus Using Programmable Biomolecular Components. *Cell* **165**, 1255-1266, (2016).

4 Sachdeva, G., Garg, A., Godding, D., Way, J. C. & Silver, P. A. In vivo co-localization of enzymes on RNA scaffolds increases metabolic production in a geometrically dependent manner. *Nucleic Acids Res.* **42**, 9493-9503, doi:10.1093/nar/gku617 (2014).

APPENDIX A

COPYRIGHT PERMISSIONS FOR ADAPTIONS OF FIGURES

A Simple Fluorescent Biosensor for Theophylline Based on its RNA Aptamer

Author: C. J. Rankin, , E. N. Fuller, et al

Publication: Nucleosides, Nucleotides, and Nucleic Acids

Publisher: Taylor & Francis

Date: Oct 1, 2006

Thesis/Dissertation Reuse Request

Taylor & Francis is pleased to offer reuses of its content for a thesis or dissertation free of charge contingent on resubmission of permission request if work is published.

BACK CLOSE

Detection of Bioactive Small Molecules by Fluorescent Resonance Energy Transfer (FRET) in RNA–Protein Conjugates

Author: Tamaki Endoh, Ryo Shintani, Masayasu Mie, et al

Publication: Bioconjugate Chemistry

Publisher: American Chemical Society

Date: Dec 1, 2009